

Review

Searches for Lepton Flavor Violation in Tau Decays at Belle II

Swagato Banerjee 

Department of Physics and Astronomy, University of Louisville, Louisville, KY 40292, USA;
swagato.banerjee@louisville.edu

Abstract: Searches for lepton flavor violation in tau decays are unambiguous signatures of new physics. The branching ratios of tau leptons at the level of 10^{-10} – 10^{-9} can be probed using 50 ab^{-1} of electron-positron annihilation data being collected by the Belle II experiment at the world's highest luminosity accelerator, the SuperKEKB, located at the High Energy Accelerator Research Organization, KEK, in Tsukuba, Japan. Searches with such expected sensitivity will either discover new physics or strongly constrain several new physics models.

Keywords: lepton flavor violation; new physics in tau decays; B-Factor; Belle II experiment

1. Introduction

Lepton flavor conservation stands out in the Standard Model (SM) among all other symmetries because it is not associated with any underlying conserved current. Lepton flavor violation (LFV) in the charged sector is predicted by many new physics (NP) models. The small but finite mass of the neutrinos in the SM allow charged LFV in neutrino-less two-body decays, e.g., $\tau^- \rightarrow \ell_i^- \gamma$ decays (charge conjugate modes are implied throughout the text, unless otherwise specified), where ℓ_i^- ($i = 1, 2$) denotes light charged leptons (e^- , μ^-). However, such decays are suppressed by a factor of $(m_\nu^2/m_W^2)^2$ [1], which produces experimentally unreachable rates of the order of 10^{-54} . For neutrino-less three-body decays, e.g., $\tau^- \rightarrow \ell_i^- \ell_j^+ \ell_a^-$ decays (where $a = i$ or j , and i may or may not be equal to j), two conflicting predictions existed in the literature: one of the order of 10^{-55} [2] and another of the order of 10^{-14} [3]. Recently, the contributions due to finite neutrino masses for such decays were re-scrutinized and found to be in the range of $[10^{-56}, 10^{-54}]$ [4,5], thereby laying to rest the claim that such decays could be of the order of 10^{-14} in the SM. Thus, any observation of charged LFV is an unambiguous signature of NP.

A discovery of LFV in the charged sector may provide deeper insight into several unsolved mysteries such as the origin of the dark sector, large baryon number asymmetry, number of flavor generations and extra dimensions. Many NP models, such as low-scale seesaw models [6], supersymmetric standard models [7–13], little Higgs models [14,15], leptoquark models [16], non-universal Z' models [17], and extended Higgs models [18–22], predict LFV in τ decays at the level of 10^{-10} – 10^{-8} which are just below the current experimental bounds. Predictions for two-body and three-body neutrino-less τ decays from some of these NP models [6–11,13,17] are tabulated in Table 1.

arXiv:2209.11639v1 [hep-ex] 23 Sep 2022



Citation: Banerjee, Sw. Searches for Lepton Flavor Violation in Tau Decays at Belle II. *Universe* **2022**, *8*, 480. <https://doi.org/10.3390/universe8090480>

Academic Editors: Robert H. Bernstein and Bertrand Echenard

Received: 11 April 2022

Accepted: 18 August 2022

Published: 13 September 2022

Publisher's Note: MDPI stays neutral with regard to jurisdictional claims in published maps and institutional affiliations.



Copyright: © 2022 by the author. Licensee MDPI, Basel, Switzerland. This article is an open access article distributed under the terms and conditions of the Creative Commons Attribution (CC BY) license (<https://creativecommons.org/licenses/by/4.0/>).

Table 1. The branching fractions (\mathcal{B}) for $\tau^- \rightarrow \ell^- \gamma$ and $\tau^- \rightarrow \ell^- \ell^+ \ell^-$ decays in some NP models.

	$\mathcal{B}(\tau^- \rightarrow \ell^- \gamma)$	$\mathcal{B}(\tau^- \rightarrow \ell^- \ell^+ \ell^-)$
SM + seesaw [6]	10^{-9}	10^{-10}
SUSY + Higgs [9,10]	10^{-10}	10^{-8}
SUSY + SO(10) [11,13]	10^{-8}	10^{-10}
Non-universal Z' [17]	10^{-9}	10^{-8}

Since τ is the only lepton that can decay hadronically, many neutrino-less final states are allowed via LFV processes in NP models within the observable parameter space [23]. Example of such processes include final states containing a light lepton and a meson e.g., $\tau^- \rightarrow \ell^- M^0$ (where $M^0 = \pi^0, K_S^0, \eta, \rho^0, \omega, K^{*0}, \bar{K}^{*0}, \eta', a_0, f_0, \phi$), or a light lepton and two mesons: $\tau^- \rightarrow \ell^- h^+ h^-, \ell^+ h^- h^-, \ell^- h^0 h^0$ (where $h^\pm = \pi^\pm / K^\pm, h^0 = \pi^0 / K_S^0$).

Searches for all possible LFV processes in decays of τ are necessary because there are strong correlations between the expected rates of the different channels in various models. For example, in some supersymmetric seesaw models [24,25], the relative rates of $\mathcal{B}(\tau^\pm \rightarrow \mu^\pm \gamma) : \mathcal{B}(\tau^\pm \rightarrow \mu^\pm \mu^+ \mu^-) : \mathcal{B}(\tau^\pm \rightarrow \mu^\pm \eta)$ are predicted to have specific ratios, depending on the model parameters. In the unconstrained minimal supersymmetric model, which includes various correlations between the τ and μ LFV rates, the LFV branching fractions of the τ lepton in some decay channels can be as high as 10^{-8} [26,27]), while still respecting the strong experimental bounds on the LFV decays of the μ lepton [28,29]. Thus, it is critical to probe all possible LFV modes of the τ lepton, because any excess in a single channel will not provide sufficient information to nail down the underlying LFV mechanism or even to identify an underlying theory.

More exotic decay modes, such as $\tau^- \rightarrow \pi^+ \ell^- \ell^-$ and $K^+ \ell^- \ell^-$, accompanied by a violation of the lepton number (LNV), are predicted at the level of 10^{-10} – 10^{-8} in several scenarios beyond the SM [30]. Several of these decay modes are expected to have branching ratios close to existing experimental limits in NP models, e.g., heavy Dirac neutrinos [31,32], supersymmetric processes [25,33], flavor-changing Z' exchanges with non-universal couplings [34], etc., to name a few. Wrong-sign $\tau^- \rightarrow \ell_i^+ \ell_j^- \ell_j^-$ decays are very intriguing because they are expected at rates only one order of magnitude below the present bounds in some NP models, e.g., the Littlest Higgs model with T-parity realizing an inverse seesaw [35].

Most models for baryogenesis, a hypothetical physical process based on different descriptions of the interaction between the fundamental particles that took place during the early universe producing the observed matter–antimatter asymmetry, require baryon number violation (BNV), which in charged lepton decays automatically implies LNV and LFV [36]. Angular momentum conservation requires the difference of net baryon number (B) and lepton number (L) to be equal to either 0 or 2. Although the SM conserves this difference, the symmetry group for the sum of baryon number and lepton number can be associated with an anomalous current. A set of models predicts baryogenesis that conserves B-L but includes instanton induced B+L violating currents [37]. In a large class of models [38], BNV in τ decay modes containing baryons in the final state, for example, $\tau^- \rightarrow \pi^- \Lambda, \pi^- \bar{\Lambda}, K^- \Lambda, K^- \bar{\Lambda}, \bar{p} \gamma, \bar{p} \ell_i \bar{\ell}_j$ and $p \ell_i \ell_j$, are predicted at observable rates in the large τ data set that the Belle II detector will record over the coming years.

2. Belle II Experiment at SuperKEKB

The most restrictive limits on LFV in τ decays at the level of 10^{-8} have been obtained by the first generation of the B-Factory experiments, Belle and *BABAR*, where a big data sample of τ^- ’s was generated thanks to large and similar values of the production cross-sections of B –mesons and τ^- pairs around the $Y(4S)$ resonance at the level of a nanobarn (nb) [39]. Belle

and *BABAR* experiments collected approximately one attobarn-inverse (ab^{-1}) and half an ab^{-1} of e^-e^+ annihilation data, respectively. The next generation of the B-Factory experiment, Belle II, is expected to collect $50 ab^{-1}$ of data over the next decade [40]. Such a huge data sample corresponding to 10^{11} single τ -decays would lower the limits on LFV in τ decays by one or two orders of magnitude.

2.1. Luminosity Upgrade of SuperKEKB

The asymmetric beam energy e^-e^+ collider, SuperKEKB, is an upgrade of the KEKB accelerator facility in Tsukuba, Japan, and has a circumference of about 3 km. The main components of the SuperKEKB collider complex are a 7 GeV electron ring known as the high-energy ring (HER), a 4 GeV positron ring known as the low-energy ring (LER), and an injector linear accelerator with a 1.1 GeV positron damping ring [41]. The HER and the LER have four straight sections named Tsukuba, Oho, Fuji, and Nikko, with the interaction point in the straight section of Tsukuba, where the Belle II detector is located.

The target integrated luminosity of $50 ab^{-1}$ to be collected by the Belle II experiment will be achieved by increasing the instantaneous luminosity by a factor of 30. Two major upgrades account for this increase: a modest two-fold increase in the beam currents, and a fifteen-fold reduction of the vertical beta function at the interaction point (β_y^*) from 5.9 mm to 0.4 mm, according to the “nano-beam” scheme described below.

Compared to KEKB, the asymmetry between the beam energies for the HER/LER beams were reduced from 8.0/3.5 GeV to 7.0/4.0 GeV, which reduces the beam loss due to Touschek scattering. This also improves the solid-angle acceptance of the experiment, which helps to analyze events with large missing energy. Additionally, the effects of synchrotron radiation as a result of higher currents are mitigated. Since synchrotron radiation is proportional to the product of beam current and the fourth power of beam energy, the HER at SuperKEKB emits $(7/8)^4 = 59\%$ as much synchrotron radiation per unit of beam current compared to KEKB [42]. This facilitates the SuperKEKB collider to operate at a beam current twice the value of the KEKB.

The very high luminosity environment of SuperKEKB required significant upgrades of the injection beams with high current and low emittance. The upgraded accelerator complex houses a new electron-injection gun and a new target for positron production. A new damping ring was installed for injection of the positron beam with low-emittance, as well as for improving simultaneous top-up injections needed for the high luminosity upgrade. The upgrade also features completely redesigned lattices for the LER and HER, replacement of short dipoles with longer ones in the LER, a new Titanium Nitride coated beam pipe with antechambers to suppress the electron-cloud effect, a modified RF system, and a completely redesigned interaction region [43].

The design of the beam parameters at SuperKEKB [44] follows the “nano-beam” and the “crab-waist” schemes, which were originally proposed for the SuperB-Factory in Italy [45]. Accordingly, the transverse sizes of the beam bunches in the horizontal plane (σ_x) are squeezed to have very small values and made to collide at a larger horizontal crossing angle ($2\phi_x$) = 83 mrad at Belle II, instead of =22 mrad at Belle. Thus, the effective size of the overlap region ($\tilde{\sigma}_z$) is much shorter than what it would have been in the case of a normal head-on collision, which is given by the longitudinal size of the beam bunches in the horizontal plane (σ_z) [46].

The vertical beta function at the interaction point (IP) is constrained due to the hour-glass effect as: $\beta_y^* > \tilde{\sigma}_z = \frac{\sigma_x^*}{\sin\phi_x} = \frac{\sigma_z}{\Phi}$, where Φ is the large Piwinski angle. With σ_z of the order of 6 mm, the β_y^* is thus squeezed down to about 400 μm , which is much shorter than the real bunch length. In addition to increasing the luminosity, a reduction of the interaction region of the colliding beams restricts the vertex position along the beam axis, thus providing an additional

benefit of more precise estimation of the primary vertex, which helps in the reconstruction of the complete event topology during physics analysis.

The instantaneous luminosity in an e^-e^+ collider is

$$\mathcal{L} = \frac{N_{e^-} N_{e^+} f}{4\pi\sigma_x^* \sigma_y^*} R_{\mathcal{L}},$$

where N_{e^-} is the number of electrons per bunch, N_{e^+} is the number of positrons per bunch, f is the collision frequency of the bunch, σ_x^* and σ_y^* are the transverse beam-profile sizes at the IP, and $R_{\mathcal{L}}$ is the luminosity-reduction factor (of the order of unity) due to the finite beam-crossing angle. In terms of beam currents $I_{\pm} = N_{e^{\pm}} e f$, the luminosity becomes

$$\mathcal{L} = \frac{N_{e^{\mp}} I_{e^{\pm}}}{e} \frac{1}{4\pi} \frac{R_{\mathcal{L}}}{\sigma_x^* \sigma_y^*},$$

where e is the charge of the electron. Each beam affects the stability of the other, which can be characterized by the beam–beam tune shift parameters given by

$$\zeta_{(x,y)}^{\pm} = \frac{r_e}{2\pi\gamma_{\pm}} \frac{N_{e^{\mp}} \beta_{(x,y)}^*}{\sigma_{(x,y)}^* (\sigma_x^* + \sigma_y^*)} R_{\zeta_{(x,y)}^{\pm}},$$

where r_e is the classical radius of the electron, γ_{\pm} is the relativistic gamma factor of e^- (e^+) beams, and $R_{\zeta_{(x,y)}^{\pm}}$ is the geometric reduction factor (also of the order of unity) due to the hour-glass effect. Putting all these factors altogether, we arrive at the following expression for instantaneous luminosity:

$$\mathcal{L} = \frac{\gamma_{\pm}}{2er_e} \left(1 + \frac{\sigma_y^*}{\sigma_x^*}\right) \frac{I_{e^{\pm}} \zeta_y^{\pm}}{\beta_y^*} \left(\frac{R_{\mathcal{L}}}{R_{\zeta_{(x,y)}^{\pm}}}\right),$$

where the design parameters for beam–beam tune shifts are $\zeta_{(x,y)} = (0.0012, 0.0807)$ for HER and $= (0.0028, 0.0881)$ for LER [44]. The horizontal/vertical beam sizes at the IP are reduced from $\sigma_x^*/\sigma_y^* = 170 \mu\text{m}/940 \text{ nm}$ for HER and $=147 \mu\text{m}/940 \text{ nm}$ for LER at Belle to $=10.7 \mu\text{m}/62 \text{ nm}$ for HER and $=10.1 \mu\text{m}/48 \text{ nm}$ for LER at Belle II, respectively [41]. The beam currents for Belle were 1.19 A and 1.64 A for HER and LER, respectively, compared to the design values of 2.6 A and 3.6 A for HER and LER, respectively, at Belle II [41]. This allows one to improve upon the value of instantaneous luminosity from $\mathcal{L} = 2.1 \times 10^{34} \text{ cm}^2\text{s}^{-1}$ at Belle to $6.5 \times 10^{35} \text{ cm}^2\text{s}^{-1}$ at Belle II [40].

2.2. Detector Upgrade of Belle II

From the IP outward, the main components of the Belle II detector are vertexing and tracking detectors, particle identification systems, calorimeter and muon chambers, as shown in Figure 1 [47]. The tracking detectors consist of an inner Silicon PiXel Detector (PXD), a Silicon Vertex Detector (SVD) and a Central Drift Chamber (CDC). Two dedicated particle identification systems are the Time-Of-Propagation (TOP) detector in the barrel region and the Aerogel Ring-Imaging Cherenkov detector (ARICH) in the forward endcap. These are surrounded by an Electromagnetic Calorimeter (ECL) and a superconducting solenoid providing a homogeneous magnetic field of 1.5 T. A K_L^0 and Muon detector (KLM) is the largest and outermost part of the Belle II detector.

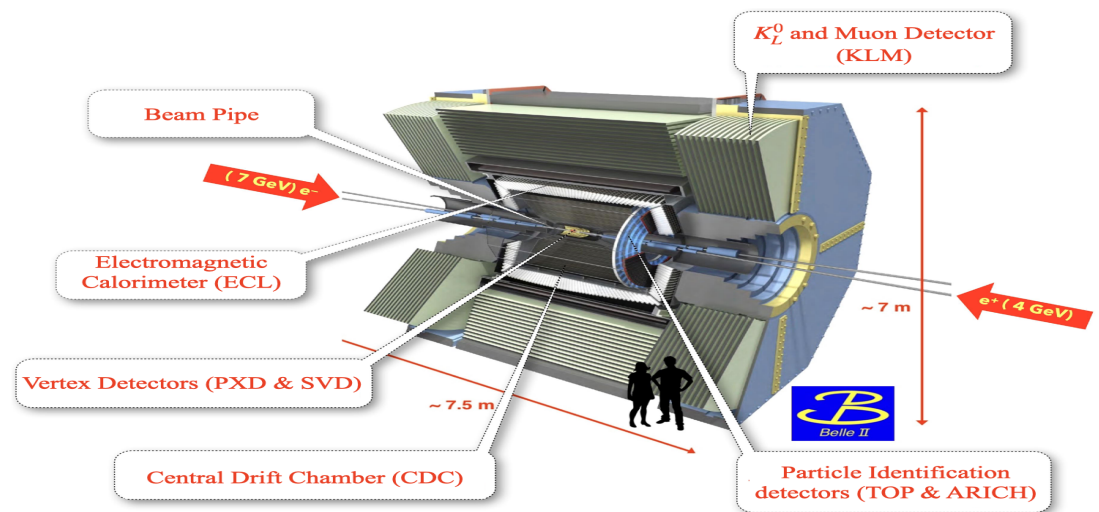


Figure 1. Schematic view of the Belle II detector [47]. The self-annotated figure is based on overview available from SuperKEKB/Belle II public page: https://www.belle2.org/project/super_kekb_and_belle_ii (accessed on 11 April 2022). Picture copyright and credit: KEK.

Some upgrades of the Belle II detector [47,48] over the Belle detector [49] are:

- **Vertexing:**
In Belle, the beam pipe was at 15 mm [50], the innermost layer of a 4-layer silicon vertex detector [51] was at 20 mm and the outermost layer of the vertex detector was at a radius of 88 mm. In Belle II, the beam pipe is at 10 mm, the inner two layers of the PXD, consisting of silicon pixels, are closer to the IP at 14 mm and 22 mm, respectively, and the outermost layer of the four layers of the SVD, consisting of silicon strips, goes to a larger radius of 140 mm. The PXD is based on the Depleted Field Effect Transistor (DEPFET) technology, which allows for thin sensors with 50 μm thickness. The readout of the new silicon strip detector is based on the APV25 chip, which has a much shorter shaping time to accommodate for higher background rates in Belle II than the VAITA chip-based readout used at Belle. As a result of these upgrades, considerably better performance is expected in Belle II than Belle. For example, the vertex resolution at Belle II is improved by the excellent spatial resolution of the two innermost pixel detector layers.
- **Tracking:**
The large volume CDC at Belle II, with 56 layers organized in 9 super-layers, has smaller drift cells than in Belle. CDC starts just outside the expanded silicon strip detector, and extends to a larger radius of 1130 mm in Belle II as compared to 880 mm in Belle. The measured spatial resolution of the CDC is about 100 μm , while the relative precision of the dE/dx measurement for particles with an incident angle of 90° is around 12%. The angular resolution achieved between tracks is ~ 4.5 mrad. The efficiency to reconstruct $K_S^0 \rightarrow \pi^- \pi^+$ decays in Belle II is also improved because the silicon strip detector occupies a larger volume.
- **Particle Identification:**
Belle II has two completely new, more compact particle identification devices of the Cherenkov imaging type: TOP in the barrel and ARICH in the endcap regions. Both detectors are equipped with very fast read-out electronics, leading to very good kaon versus pion separation in the kinematic limits of the experiment. The two Cherenkov detectors are designed to differentiate between K and π particles over the entire momentum range, and also differentiates among π , μ , and e below 1 GeV/c.

- **Calorimetry:**
The ECL is made of CsI(Tl) scintillation crystals of size 6 cm × 6 cm each with high light output, a short radiation length, and good mechanical properties, covering the range of $12^\circ < \theta < 155^\circ$ in the polar angle, e.g., 90% of solid angle coverage in the center-of-mass system. The ECL is divided into two parts: the barrel and the endcap. While the barrel part consists of 6624 crystals, the endcap part consists of 2112 crystals. The new electronics of the ECL are of the wave-form-sampling type, which has particular relevance in missing-energy studies by reducing the noise due to pile up considerably. The ECL is able to detect neutral particles in a wide energy range, from 20 MeV up to 4 GeV, with a high resolution of $\sigma_E/E = 4\%$ at 100 MeV, and angular resolution of 13 mrad (3 mrad) at low (high) energies. This gives a mass resolution for reconstructing $\pi^0 \rightarrow \gamma\gamma$ of about $4.5 \text{ MeV}/c^2$ [52].
- **K_L^0 and Muon Detection:**
The K_L^0 and muon detector (KLM) at Belle was based on glass-electrode resistive plate chambers (RPC). Since larger backgrounds are expected in the high luminosity environment at Belle II, the upgraded KLM system consists of RPC only in some parts of the barrel. The two innermost layers in the barrel and the entire endcap section of KLM at Belle II consist of layers of scintillator strips with wavelength shifting fibers, read out by silicon photomultiplier (SiPMs) as light sensors [53]. Although the high neutron background can cause damage to the SiPMs, the upgraded KLM has been demonstrated to operate reliably during irradiation tests by appropriately setting the discrimination thresholds.

2.3. Daq Upgrade of Belle II

The new data acquisition (DAQ) system [54] meets the requirements of considerably higher event rates at Belle II. It consists of a Level One (L1) [55] and High Level Trigger (HLT). The L1 trigger has a latency of 5 μs and a maximum trigger output rate of 30 kHz, limited by the read-in rate of the DAQ. The HLT must suppress online event rates to 10 kHz for offline storage using complete reconstruction with all available information from the entire detector. To enable readout from high-speed data transmission, a peripheral component interconnect express based readout module (PCIe40) with high data throughput of up to 100 Gigabytes/s was adopted for the upgrade of the Belle II DAQ system [56]. The trigger system at Belle II achieves almost 100 % trigger efficiency for $Y(4S) \rightarrow B\bar{B}$ events and nearly high efficiency for other physics processes of interest, e.g., τ -pair events.

3. Search Strategies

3.1. Event Topology

B-Factories typically operate at center-of-mass energies around the $Y(4S)$ resonance, e.g., 10.58 GeV. Tau-pair production via e^-e^+ annihilation in this energy regime leads to cleanly separated event topology associated with the decay of each τ lepton, and are well simulated by state-of-the-art event generators: KK2F [57–59], Tauo1a [60,61] and Photos [62,63]. Searches for LFV in τ decays in B factories exploit these event characteristics, assuming that only one of the two τ 's produced in the $e^-e^+ \rightarrow \tau^-\tau^+$ process could have decayed in this rare mode, and the other τ decays via the allowed SM processes. By dividing the event into a pair of hemispheres perpendicular to the thrust axis [64,65] in the center-of-mass frame, τ decay products can thus be identified as coming from the signal-side and the tag-side, corresponding to decay via LFV and the SM decays of the τ lepton, respectively.

3.2. Signal Characteristics

The characteristic feature of τ decays via LFV is that the final state does not contain ν_τ . Thus, there is no missing momentum associated with the signal-side, and the kinematics of the

signal τ lepton can be completely reconstructed from measurements of the final state particles. Simulation studies for more than a hundred possible decays via LFV that can be searched with such signal characteristics for each sign of the τ lepton, are possible with recent updates of the Tauola event generator [61,66,67], which have been seamlessly integrated into the software of the Belle II experiment.

A very interesting feature of τ -pair production in e^-e^+ annihilation is that the energy of each τ lepton is known to be exactly half of the center-of-mass (CM) energy of the collision, except for corrections due to initial and final state radiations. Therefore, the uncertainty of the energy of the τ lepton is independent of the performance of the detector, and is known from the beam energy spread of SuperKEKB to be approximately 5 MeV [48].

As a first example of the signal mode, let us consider $\tau^- \rightarrow \ell^- \gamma$ decays, which are predicted with rates just lower than the current experimental bounds in the widest variety of NP models and are hence regarded as “golden modes” in searches for LFV. The total energy in the CM frame of the τ decay products in the signal-side is $E_{\ell\gamma}^{\text{CM}} = \sqrt{s}/2$, and the invariant mass of the $\ell\gamma$ pair can be calculated as $m_{\ell\gamma} = 2\sqrt{p_\ell E_\gamma} \sin(\frac{\theta}{2})$, where p_ℓ is the magnitude of the three-momentum of the lepton, E_γ is the energy of the photon, and θ is the opening angle between them. The invariant mass is ideal as a discriminating variable, because its resolution is given by [68]:

$$\frac{\Delta m_{\ell\gamma}}{m_{\ell\gamma}} = \frac{1}{2} \sqrt{\left(\frac{\Delta p_\ell}{p_\ell}\right)^2 + \left(\frac{\Delta E_\gamma}{E_\gamma}\right)^2 + \left(\frac{\Delta\theta}{\tan\frac{\theta}{2}}\right)^2}$$

which simultaneously combines all the available experimental precision on the measured energy/momentum from the calorimeter/tracking systems with the measured uncertainties on the position measurements of the observable final state decay products. The resolution of this kinematic variable is further improved by considering the beam-energy-constrained mass, M_{bc} , given as:

$$M_{\text{bc}} = \sqrt{(E_{\text{beam}}^{\text{CM}})^2 - |\vec{p}_{\ell\gamma}^{\text{CM}}|^2},$$

where $E_{\text{beam}}^{\text{CM}} = \sqrt{s}/2$ and $\vec{p}_{\ell\gamma}^{\text{CM}}$ is the sum of the lepton and photon momenta in the CM frame, because the resolution of $E_{\text{beam}}^{\text{CM}}$ comes from the accelerator instead of the detector.

The beam-energy-constrained τ mass, labeled somewhat differently as m_{EC} for the BABAR search [69], is typically obtained from a kinematic fit that constrains the CM energy of the τ to be $\sqrt{s}/2$. Its resolution was further improved in the BABAR search by assigning the origin of the photon candidate to the point of the closest approach of the signal lepton track to the e^-e^+ collision axis. Figure 2 shows a comparison study using a simulated sample of signal $\tau^- \rightarrow \mu^- \gamma$ events, where the resolution of the invariant mass is crudely estimated to be 18.2 MeV/ c^2 from a single Gaussian fit to the peak of the distribution, while that of m_{EC} is 12.1 MeV/ c^2 , which improves further to 8.3 MeV/ c^2 after the vertex constraint.

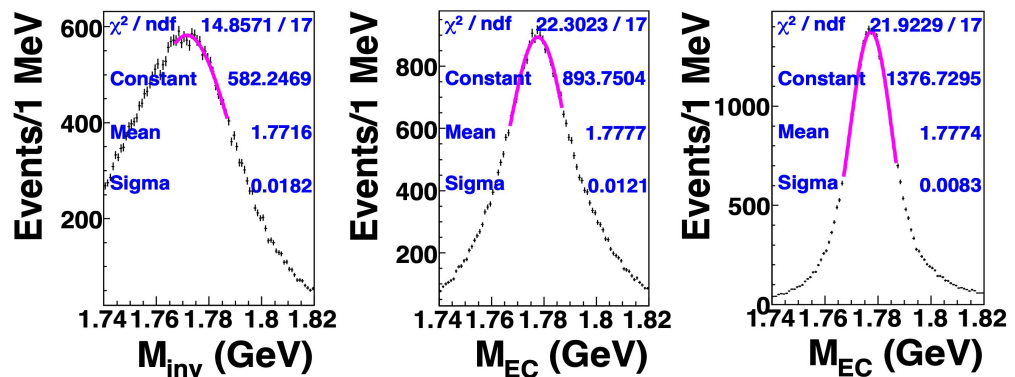


Figure 2. Invariant mass (left), m_{EC} without vertex constraint (middle) and m_{EC} with vertex constraint (right) obtained from simulated samples during analysis strategy development studies for $\tau^- \rightarrow \mu^- \gamma$ search at the *BABAR* experiment [69].

The most distinguishing feature of signal events is obtained by considering the characteristic mass of the decay products of the LFV τ decays along with the normalized difference in their energy from half the center-of-mass energy in $e^- e^+$ annihilation, so that the search can be uniformly performed at energies other than the $Y(4S)$ peak, to take advantage of the larger luminosity including all the recorded data:

$$\Delta E/\sqrt{s} = (E_{\ell\gamma}^{CM} - \sqrt{s}/2)/\sqrt{s}.$$

The signal events are clustered around $M_{bc} \sim m_\tau$ and $\Delta E/\sqrt{s} \sim 0$ in the two-dimensional plots of ΔE vs. M_{bc} , as shown in Figures 3 and 4 for $\tau^- \rightarrow e^- \gamma$ (left) and $\tau^- \rightarrow \mu^- \gamma$ (right) searches at Belle [70] and *BABAR* [69] experiments, respectively, where the variable m_{EC} refers to the beam-energy-constrained mass in the latter, as mentioned earlier.

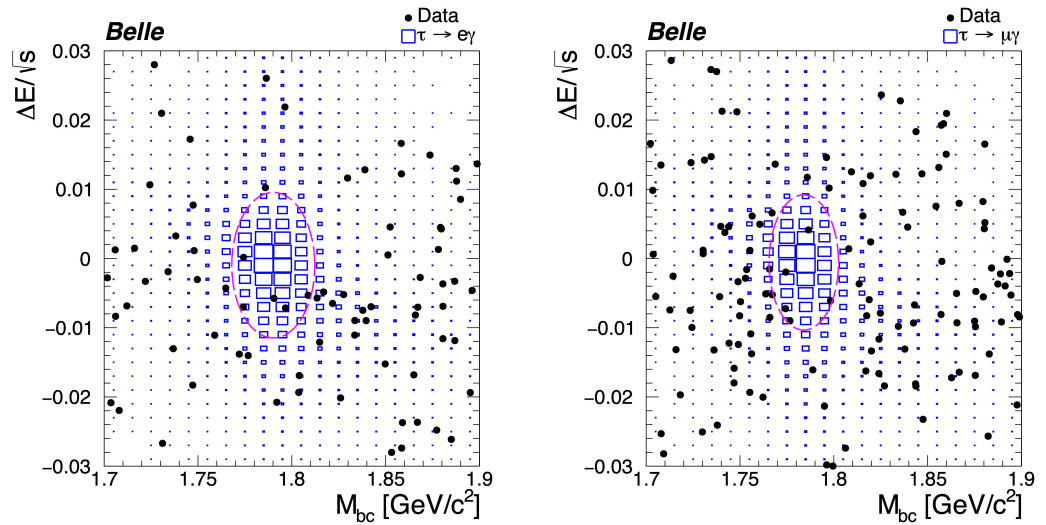


Figure 3. Two-dimensional distributions of $\Delta E/\sqrt{s}$ versus M_{bc} for Belle searches [70] for $\tau^- \rightarrow e^- \gamma$ (left) and $\tau^- \rightarrow \mu^- \gamma$ (right) decays. Black points are data, blue squares are $\tau^- \rightarrow \ell^- \gamma$ signal MC events, and magenta ellipses show the signal region ($\pm 2\sigma$ region). This figure has been reprinted with permission from Ref. [70].

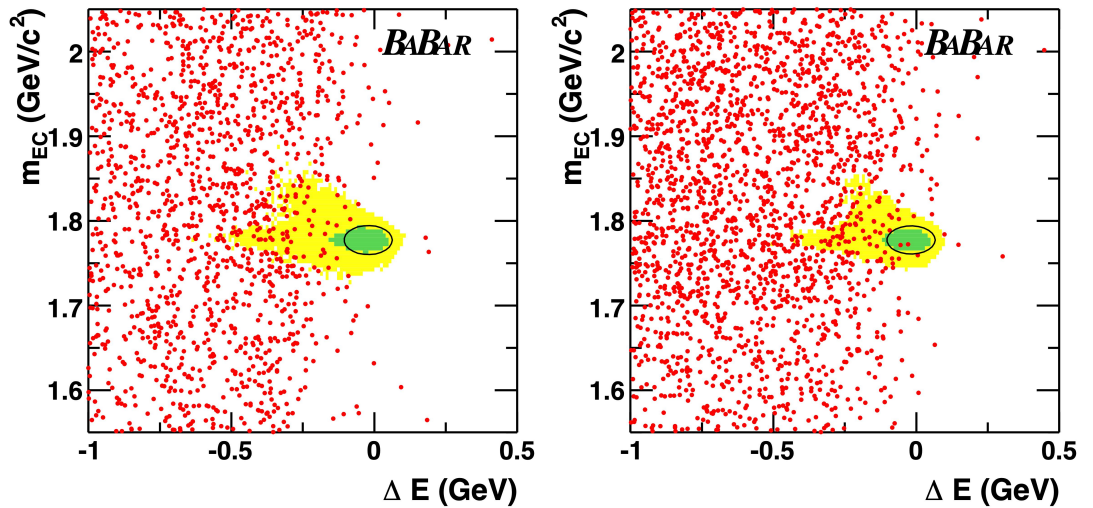


Figure 4. Two-dimensional distributions in the m_{EC} vs. ΔE plane for the *BABAR* searches [69] for $\tau^- \rightarrow e^- \gamma$ (left) and $\tau^- \rightarrow \mu^- \gamma$ (right) decays. Data are shown as dots and contours containing 90% (50%) of signal MC events are shown as light-yellow (dark-green) shaded regions, along with the 2σ contours shown as black ellipses. This figure has been reprinted with permission from Ref. [69].

All analyses are developed in a blind manner, e.g., optimizing the event selection before looking at the data events inside the signal region, to avoid experimental bias in the search for LFV τ decays. The search sensitivity can be optimized to give the smallest expected upper limit in the background-only hypothesis inside a 2σ ellipse, for example, amongst other possible choices. A typical 2σ signal region is defined as the following elliptical regions:

$$\frac{(M_{bc} - \mu_{M_{bc}})^2}{(2\sigma_{M_{bc}})^2} + \frac{(\Delta E/\sqrt{s} - \mu_{\Delta E/\sqrt{s}})^2}{(2\sigma_{\Delta E/\sqrt{s}})^2} < 1.0,$$

$$\sigma_{M_{bc}} = 0.5(\sigma_{M_{bc}}^{\text{high}} + \sigma_{M_{bc}}^{\text{low}}),$$

$$\sigma_{\Delta E/\sqrt{s}} = 0.5(\sigma_{\Delta E/\sqrt{s}}^{\text{high}} + \sigma_{\Delta E/\sqrt{s}}^{\text{low}}).$$

Here, $\sigma_{M_{bc}}^{\text{high/low}}$ and $\sigma_{\Delta E/\sqrt{s}}^{\text{high/low}}$ are the widths on the higher/lower side of the peak obtained by fitting the signal distribution to an asymmetric Gaussian function [71].

For the Belle search [70], the resolutions are $\sigma_{M_{bc}}^{\text{high/low}} = 11.55 \pm 0.27/10.59 \pm 0.19$ MeV/ c^2 and $\sigma_{\Delta E/\sqrt{s}}^{\text{high/low}} = (6.1 \pm 0.7)/(4.4 \pm 0.3) \times 10^{-3}$ for $\tau^- \rightarrow e^- \gamma$ events; and $\sigma_{M_{bc}}^{\text{high/low}} = 11.08 \pm 0.08/7.46 \pm 0.23$ MeV/ c^2 and $\sigma_{\Delta E/\sqrt{s}}^{\text{high/low}} = (5.6 \pm 0.4)/(4.2 \pm 0.2) \times 10^{-3}$ for $\tau^- \rightarrow \mu^- \gamma$ events. The mean values are $\langle M_{bc} \rangle = 1.79$ MeV/ c^2 and $\langle \Delta E/\sqrt{s} \rangle = -1.0 \times 10^{-3}$ for $\tau^- \rightarrow e^- \gamma$ events, and $\langle M_{bc} \rangle = 1.78$ MeV/ c^2 and $\langle \Delta E/\sqrt{s} \rangle = -0.6 \times 10^{-3}$ for $\tau^- \rightarrow \mu^- \gamma$ events. For the *BABAR* search [69], the resolutions for m_{EC} and ΔE are 8.6 MeV/ c^2 and 42.1 MeV for $\tau^- \rightarrow e^- \gamma$, and 8.3 MeV/ c^2 and 42.2 MeV for $\tau^- \rightarrow \mu^- \gamma$, respectively, centered on 1777.3 MeV/ c^2 and -21.4 MeV for $\tau^- \rightarrow e^- \gamma$, and 1777.4 MeV/ c^2 and -18.3 MeV for $\tau^- \rightarrow \mu^- \gamma$. Shifts from zero for $\langle \Delta E \rangle$ are mostly due to initial and final state radiations.

The mass and energy kinematic variables typically have a small correlation arising from initial and final state radiation, as well as energy/momentum scale calibration effects. For the *BABAR* search [69], the correlation was estimated to be -8.5% and -8.4% for the $\tau^- \rightarrow e^- \gamma$ and

$\tau^- \rightarrow \mu^- \gamma$ decays, respectively, around the core region. Without the beam-energy constraint, the correlation between the invariant mass and energy variables are typically much higher.

LFV process in τ decays containing a resonance in the final state are identified by the presence of a peak in the invariant mass of the daughter particles in the simulation of the signal process. For example, distributions of invariant mass of the $\pi^+ \pi^-$, $K^+ K^-$, $\pi^+ \pi^- \pi^0$, $K^+ \pi^-$, $\pi^+ K^-$ and $\pi^+ \pi^-$ systems in the signal-side are studied and confirmed to contain the respective resonances in searches for $\tau^- \rightarrow \mu^- \rho^0$, $\tau^- \rightarrow \mu^- \phi$, $\tau^- \rightarrow \mu^- \omega$, $\tau^- \rightarrow \mu^- K^{*0}$, $\tau^- \rightarrow \mu^- \bar{K}^{*0}$ and $\tau^- \rightarrow \mu^- f_0(980)$ decays, respectively, performed by the Belle experiment [72,73]. The selected mass regions ensure that the signal is unambiguously selected in the corresponding searches.

3.3. Background Suppression

Background events containing leptons from decays of heavy quarks are easily suppressed by appropriate cuts on Fox-Wolfram moments [74], and on the invariant mass of all decay products on the tag-side. The characteristic difference between τ -pairs events with LFV decays and backgrounds consisting of generic τ -pair, di-lepton, two-photon production and $q\bar{q}$ processes (where $q = u, d$ or s), in the number of neutrinos in the signal-side and tag-side, as defined by the event topology in Section 3.1, are shown in Table 2.

Table 2. Number of neutrinos in the event for signal and background processes.

# of ν 's	LFV Decays	Generic τ -Pair	Other Backgrounds
Signal-side	0	1–2	0
Tag-side	1–2	1–2	0

Since decay products of the τ decay via LFV in the signal-side do not contain any neutrino, the direction of the τ lepton in the tag-side can be precisely obtained in the center-of-mass frame by reversing the total momentum of the signal-side. This allows for good kinematic reconstruction of the missing mass in the tag-side, assuming that in the CM frame, the tag-side τ momentum is opposite that of the signal-side τ momentum and that its energy is constrained to be half the center-of-mass energy. Thus, selection of events with small values of the square of the missing mass (m_v^2) in the tag-side play an important role in the suppression of the background events [70].

Additional selection criteria are also used to suppress the backgrounds in the different LFV decay modes, which are mostly accidental in nature, except in $\tau^- \rightarrow e^- \gamma$ and $\tau^- \rightarrow \mu^- \gamma$ searches. The dominant background in the searches arise from $\tau^+ \tau^-$ events decaying via the $\tau^\pm \rightarrow e^\pm \nu_e \nu_\tau$ ($\tau^\pm \rightarrow \mu^\pm \nu_\mu \nu_\tau$) channel with a photon coming from initial-state radiation or beam background. The $e^+ e^- \gamma$ and $\mu^+ \mu^- \gamma$ events are subdominant, and are estimated to contribute to <5% of the total backgrounds in the Belle search [70]. Contributions from other sources of backgrounds, such as two-photon and $q\bar{q}$ processes, are estimated to be quite small in the signal region.

Furthermore, each component of the background processes has distinctive features as visible in their respective two-dimensional distributions in the $(\Delta M, \Delta E)$ plane, where ΔM denotes the difference between the characteristic mass of the system of τ -daughters and the well-known mass of the τ -lepton = (1776.86 ± 0.12) MeV [75], and ΔE , as defined above. The shapes of the leading backgrounds in search of $\tau^- \rightarrow \mu^- \mu^+ \mu^-$ decays as performed at the BABAR experiment [76] are shown in Figure 5, where the red box indicates the rectangular boundaries of a generic region mostly populated by the signal processes. The SM $\tau\tau$ background events are generally restricted to small negative values of both ΔM and ΔE variables, because the reconstruction of signal event topology does not account for the neutrinos present in SM τ

decays. QED background events are mostly dominated by di-lepton production as the main underlying hard process and typically lie within a narrow horizontal band across the ΔM variable centered around slightly positive values of ΔE , due to the presence of a pair of extra charged particles in such events. The QCD background events from various $q\bar{q}$ processes tend to populate the plane uniformly across the ΔM variable and drop towards large values of the ΔE variable. The expected background rates inside the signal region can be obtained by fitting the observed data in the $(\Delta M, \Delta E)$ plane to a sum of probability density functions. Such data-driven estimates, based on the shapes predicted by respective simulation samples and validated by data-driven control regions, scale well with larger data statistics. Thus, the background uncertainties can be controlled in a statistical manner, which is very useful in rare searches with high luminosity data sets.

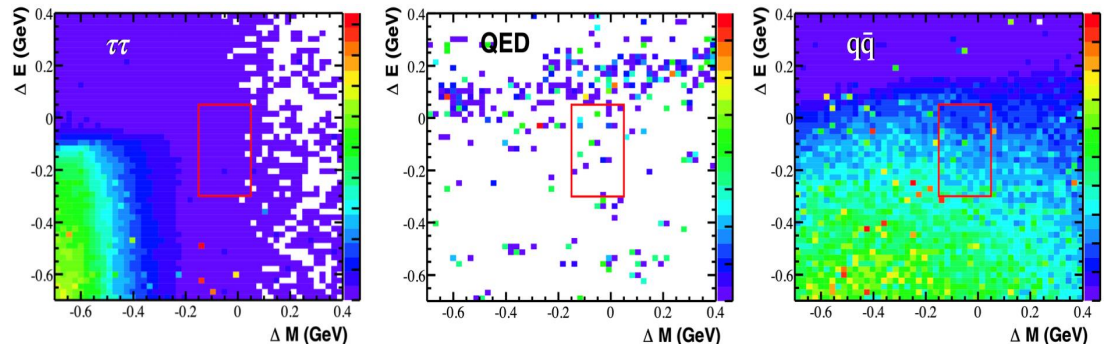


Figure 5. Two-dimensional distributions for $\tau\tau$, QED, and $q\bar{q}$ background processes in the $(\Delta M, \Delta E)$ plane obtained from simulated samples during analysis strategy development studies for $\tau^- \rightarrow \mu^- \mu^+ \mu^-$ search at the *BABAR* experiment [76]. Rectangular box-shaped regions mostly populated by the signal processes are shown in red.

3.4. Upper Limit Estimation

No excess of events has ever been observed in searches for LFV in τ decays. The upper limit at 90% confidence level (CL) on signal branching fraction (\mathcal{B}_{UL}^{90}) is calculated as:

$$\mathcal{B}_{UL}^{90} = \frac{S_{UL}^{90}}{2N_{\tau\tau}\epsilon'}$$

where $N_{\tau\tau}$ is the number of τ -pairs produced, ϵ is the reconstruction efficiency of the signal decay mode, and S_{UL}^{90} is the 90% CL upper limit on number of signal events. The factor of two enters into the denominator because either one of the two τ leptons produced in the event can decay into the rare signal channel coming from LFV.

3.4.1. Number of τ -Pairs Produced

$N_{\tau\tau}$ is obtained by summing over the product of luminosity (\mathcal{L}) and the τ -pairs production cross-section ($\sigma_{\tau\tau}$) at each of the center-of-mass energies (\sqrt{s}) where the search is conducted. The cross-section of τ -pair production in e^-e^+ annihilation follows a characteristic $1/s$ dependence, but receives additional contribution from decays of the $Y(nS)$ resonances for $n = 1, 2$ and 3 , according to the known branching fractions [75]: $\mathcal{B}(Y(1S) \rightarrow \tau^- \tau^+) = (2.6 \pm 0.1)\%$, $\mathcal{B}(Y(2S) \rightarrow \tau^- \tau^+) = (2.0 \pm 0.2)\%$ and $\mathcal{B}(Y(3S) \rightarrow \tau^- \tau^+) = (2.3 \pm 0.3)\%$. Beyond the open-beauty threshold, contributions from resonances with $n \geq 4$ are negligible.

The Belle experiment collected data with center-of-mass energies around the peak of $Y(nS)$ resonances corresponding to luminosities of 5.7 fb^{-1} , 24.9 fb^{-1} and 2.9 fb^{-1} at $n = 1, 2$ and 3 , respectively, while the *BABAR* experiment collected luminosities of 13.6 fb^{-1} and 28.0 fb^{-1} at center-of-mass energies corresponding to the $Y(nS)$ peak at $n = 2$ and 3 , respectively, as

reported in Table 3.2.1 in the reference [52]. The statistical errors on these measured luminosities are much smaller than the systematic errors, which are estimated to be 1.4% at the Belle experiment, and 0.7% (0.6%) at the BABAR experiment for $n = 2$ and 3, respectively [52].

The numbers of $Y(nS)$ produced in the Belle experiment are $(102 \pm 2) \times 10^6$, $(158 \pm 4) \times 10^6$ and $(11 \pm 0.3) \times 10^6$ for $n = 1, 2$ and 3, respectively, while in the BABAR experiment, the numbers are $(98.3 \pm 0.9) \times 10^6$ and $(121.3 \pm 1.2) \times 10^6$ for $n = 2$ and 3, respectively, as obtained from Table 3.2.2 in the reference [52]. By dividing the numbers of $Y(nS)$ resonances produced with its corresponding luminosity, the resonant production cross-sections are estimated for $Y(1S)$ to be $(17.89 \pm 0.43) nb$ in the Belle experiment, for $Y(2S)$ to be $(6.35 \pm 0.18) nb$ and $(7.23 \pm 0.08) nb$ in the Belle and BABAR experiments, and for $Y(3S)$ to be $(3.79 \pm 0.12) nb$ and $(4.33 \pm 0.05) nb$ in the Belle and BABAR experiments, respectively. For the purposes of averaging the measured values, the observed differences at $n = 2$ and 3 resonances are accounted for by calculating the PDG-style scale factors [75] $S = \sqrt{\chi^2/(N - 1)}$ equal to 4.38 and 4.24, respectively, with $N = 2$. Thus, the average values are estimated to be $(7.08 \pm 0.33) nb$ for $Y(2S)$ and $(4.24 \pm 0.20) nb$ for $Y(3S)$.

The total $\sigma_{\tau\tau}$ is obtained by adding the contributions to τ -pairs production from the continuum [39] and the contributions from the decays of the $Y(nS)$ resonances for $n = 1, 2$ and 3. The estimated values of total $\sigma_{\tau\tau}$ at the peak of $Y(nS)$ resonances and at 60 MeV below the corresponding resonances (labelled with a “—off”) are listed in Table 3.

Table 3. $\sigma_{\tau\tau}$ at different center-of-mass energies corresponding to data-taking at the B-Factories.

\sqrt{s}	$\sigma_{\tau\tau} (nb)$	\sqrt{s}	$\sigma_{\tau\tau} (nb)$
Y(1S)—off	1.142 ± 0.004	Y(1S)	1.593 ± 0.021
Y(2S)—off	1.026 ± 0.004	Y(2S)	1.157 ± 0.017
Y(3S)—off	0.966 ± 0.003	Y(3S)	1.052 ± 0.014
Y(4S)—off	0.928 ± 0.003	Y(4S)	0.919 ± 0.003
Y(5S)—off	0.881 ± 0.003	Y(5S)	0.873 ± 0.003

3.4.2. Efficiency of Signal Reconstruction

The signal reconstruction efficiency receives multiplicative reduction factors corresponding to the application of trigger, acceptance, and event topology requirements, particle identification criteria, background suppression and choice of the signal region in the two-dimensional plane given by mass versus the normalized difference of energy of the τ decay products and $\sqrt{s}/2$. At Belle and BABAR, the signal efficiencies were estimated to lie approximately between 2% to 12%, depending on the different decay channels. For example, the overall signal efficiency estimated for the search for $\tau^- \rightarrow e^- \eta'$ reconstructed via the $\eta' \rightarrow \rho(\rightarrow \pi^- \pi^+) \gamma$ and $\eta' \rightarrow \pi^- \pi^+ \eta(\rightarrow \gamma\gamma)$ decay modes is $(0.294 \times 1 \times 4.76 + 0.445 \times 0.3943 \times 4.27)\% = 2.1\%$ [77], while the search for $\tau^- \rightarrow \mu^+ e^- e^-$ decays have an efficiency of 11.5% [78]. In the Belle II experiment, an increase in the signal efficiency can be expected due to higher trigger efficiencies, improvements in the vertex reconstruction, charged track and neutral meson reconstructions, and particle identification. Refinements in the analysis techniques will produce a more accurate understanding of the physics backgrounds and would thus contribute to an increase in the signal detection efficiency, which directly translates into higher sensitivities in searches for LFV.

3.4.3. Upper Limit on the Number of Signal Events

In the case of searches with very low counts, the search becomes a single-bin counting experiment following a Poisson probability distribution, with the mean count given by the

expected number of background events (b) and possibly some signal events (s). The likelihood function (\mathcal{L}) is thus described by:

$$\mathcal{L}(s, b) = \frac{e^{-(s+b)}(s+b)^N}{N!},$$

where N is the number of observed events. If the experimental resolution of the discriminating variables allows multiple bins, the difference in shapes of the discriminating variables between the signal and background distributions can be exploited in an extended unbinned maximum likelihood fit using:

$$\mathcal{L}(s, b) = \frac{e^{-(s+b)}}{N!} \prod_{i=1}^N (s \cdot PDF_i^{sig} + b \cdot PDF_i^{bkg}),$$

where i indicates the i -th event, PDF_i^{sig} and PDF_i^{bkg} are the probability density functions (PDF) for signal and sum of all background process, respectively.

S_{UL}^{90} is obtained by considering $\mathcal{L}(s) = \int_0^\infty \mathcal{L}(s, b) db$, and integrating the likelihood $\mathcal{L}(s)$ up to the value that includes 90% of the total integral of the likelihood function, following a flat prior Bayesian prescription [79]. Alternatively, following a Frequentist prescription [80], a toy Monte Carlo approach is used to generate numerous samples with sizes that follow a Poisson distribution about the mean value being given by the number of observed events. Each sample is then fitted to obtain the number of signal and background events using the same extended unbinned maximum likelihood fit procedure as that applied to the data. S_{UL}^{90} is obtained by varying the true branching fraction of the signal such that 90% of the samples yield a fitted number of signal events greater than the number of signal events in the observed data sample. In the unified approach for finding confidence levels [81], the order of samples in the acceptance interval for a specific value of the number of signal events follows an ordering principle based on likelihood ratios, where the denominator is determined by the best fit value in each sample.

In order to have an unbiased estimate of the expected sensitivity, a blinding procedure should be followed to predict the expected background rate inside the signal region (SR), which does not depend on the observed data inside a blinding region (BR), defined as a part of a broad fit range (FR), but hiding data events inside the SR. For well-controlled modeling of the total background PDF, the number of expected background events (N_{SR}^{bkg}) inside the SR can then be estimated directly from the data N_{FR-BR}^{data} outside the blinded region using the formula:

$$N_{SR}^{bkg} = \frac{\int_{SR} PDF_{bkg}}{\int_{FR-BR} PDF_{bkg}} \times N_{FR-BR}^{data}$$

where $\int_{SR} PDF_{bkg}$ and $\int_{FR-BR} PDF_{bkg}$ are the integrals of the background probability density functions over the signal region and the non-blinded parts of the fit region.

3.5. Systematic Uncertainties

In terms of the number of τ decays being studied, $t = 2N_{\tau\tau}\epsilon$, the number of signal events are written as ($s = \mu t$), where μ is the branching fraction of the signal process and the normalization factor t includes uncertainties on luminosity, cross-section and the signal efficiency. The upper limit \mathcal{B}_{UL}^{90} including all systematic effects using the technique of Cousins and Highland [82], is calculated by propagating all the measured uncertainties onto the number of signal events (s) and background events (b).

Implementation of systematic effects in the POLE (POisson Limit Estimator) program [83] is based on the following likelihood function, which is a convolution of a Poisson distribution

with two Gaussian resolution functions corresponding to the signal normalization factor and background, as described by the following formula:

$$\mathcal{L}(\mu, t, b) = \frac{(\mu t + b)^N e^{-(\mu t + b)}}{N!} \frac{1}{2\pi\sigma_t\sigma_b} e^{-\frac{1}{2}\left(\frac{t-t}{\sigma_t}\right)^2 - \frac{1}{2}\left(\frac{b-b}{\sigma_b}\right)^2},$$

where \hat{t} and \hat{b} are the average estimates corresponding to measured uncertainties of σ_t and σ_b , respectively.

In searches for rare processes such as LFV in τ decays, often a very small number of events are expected in the signal region. Sometimes the sensitivity of the search cannot easily distinguish a very small number of signal events from the background-only hypothesis, and inappropriately tends to exclude an unusually small signal value. To overcome such difficulties, the upper limits can be calculated using the CL_s method [84,85], where the CL_s is defined as the ratio of confidence levels for the signal-plus-background hypothesis normalized by the confidence level for the background-only hypothesis. Asymptotic calculations of the likelihood ratios used as the test statistic in such methods allow for a computationally efficient estimate of the CL_s intervals [86].

A Neyman construction [87] of CL_s upper limits including systematic uncertainties is provided by the HistFactory implementation [88,89], based on the likelihood function $\mathcal{L}(\mu, \theta_j)$ defined as:

$$\mathcal{L}(\mu, \theta_j) = \prod_{\text{channel}} \prod_{\text{category}} \left[\prod_i \text{Poisson}(N_i | \mu \cdot t_i + b_i) \prod_j \text{Lognormal}(\theta_j | 0, 1) \right],$$

where N_i is the number of events observed in the i^{th} bin with signal normalization factor and background predictions given by t_i and b_i , respectively, of a multicategorical search describing, for example, different tag-side decay modes each with different sensitivity over possibly multiple decay channels of the signal mode. The systematic uncertainties are constrained by nuisance parameters θ_j corresponding to various scale factors as determined from dedicated calibration constants of efficiency measurements and are obtained from simulation studies or analysis of control regions in the data.

The HistFactory allows for the calculation of upper limits in both Bayesian and Frequentist interpretations [90], with slightly different treatments of the nuisance parameters. While in the former interpretation, the nuisance parameters are eliminated by marginalizing the posterior density, using, for example, Markov Chain Monte Carlo integration, in the latter interpretation, the nuisance parameters are determined by profiling the likelihood function based on auxiliary measurements, such as control regions, side-bands, or dedicated calibration measurements. Some uncertainties arising from theoretical calculations or ad hoc estimates are not statistical in nature and thus are not associated with auxiliary measurements. However, log-normal probability density functions of nuisance parameters are used to constrain all the uncertainties, by convention.

Bayesian limits can also be calculated using the Bayesian Analysis Toolkit [91].

4. Current Status and Future Prospects

Summary of observed limits obtained by CLEO, BABAR, Belle, ATLAS, CMS, and LHCb experiments [92] are shown in Table 4 and Figure 6, along with projections for two illustrative scenarios of luminosity $\mathcal{L} = 5 \text{ ab}^{-1}$ and 50 ab^{-1} at the Belle II experiment [40]. Projections are extrapolated from expected limits obtained at the Belle experiment. The expected limits for $\tau^- \rightarrow \ell^- \gamma$ decays are obtained from Ref. [70]. We assume the presence of irreducible backgrounds for $\tau^- \rightarrow \ell^- \gamma$ decays, thus approximating the sensitivity to upper bounds as

proportional to $1/\sqrt{\mathcal{L}}$. Given the expected number of background events in each channel from the previous searches at the Belle experiment and the improvements listed in Section 3.4.2, the background expectations corresponding to the integrated luminosity at Belle II for all other modes are still of the order of unity or less. For such accidental backgrounds, the sensitivity for upper bounds is proportional to $1/\mathcal{L}$, as discussed in Section 8.2.1.3 of Ref. [93]. The projections for the corresponding upper limits at Belle II are estimated using the Feldman and Cousins approach [81].

Table 4. Current status of observed (obs) and expected (exp) upper limits (UL) [40,75].

$\tau^- \rightarrow$	Observed Limits			Expected Limits		
	Experiment	Luminosity	UL (obs)	Experiment	Luminosity	UL (exp)
$e^- \gamma$	Belle [70]	988 fb ⁻¹	5.6×10^{-8}	Belle II [40]	50 ab ⁻¹	9.0×10^{-9}
	BABAR [69]	516 fb ⁻¹	3.3×10^{-8}			
	CLEO [94]	4.68 fb ⁻¹	2.7×10^{-6}			
$\mu^- \gamma$	Belle [70]	988 fb ⁻¹	4.2×10^{-8}	Belle II [40]	50 ab ⁻¹	6.9×10^{-9}
	BABAR [69]	516 fb ⁻¹	4.4×10^{-8}			
	CLEO [95]	13.8 fb ⁻¹	1.1×10^{-6}			
$e^- \pi^0$	Belle [77]	401 fb ⁻¹	8.0×10^{-8}	Belle II [40]	50 ab ⁻¹	7.3×10^{-10}
	BABAR [96]	339 fb ⁻¹	1.3×10^{-7}			
	CLEO [97]	4.68 fb ⁻¹	3.7×10^{-6}			
$\mu^- \pi^0$	Belle [77]	401 fb ⁻¹	1.2×10^{-7}	Belle II [40]	50 ab ⁻¹	7.1×10^{-10}
	BABAR [96]	339 fb ⁻¹	1.1×10^{-7}			
	CLEO [97]	4.68 fb ⁻¹	4.0×10^{-6}			
$e^- K_S^0$	Belle [98]	671 fb ⁻¹	2.6×10^{-8}	Belle II [40]	50 ab ⁻¹	4.0×10^{-10}
	BABAR [99]	469 fb ⁻¹	3.3×10^{-8}			
	CLEO [100]	13.9 fb ⁻¹	9.1×10^{-7}			
$\mu^- K_S^0$	Belle [98]	671 fb ⁻¹	2.3×10^{-8}	Belle II [40]	50 ab ⁻¹	4.0×10^{-10}
	BABAR [99]	469 fb ⁻¹	4.0×10^{-8}			
	CLEO [100]	13.9 fb ⁻¹	9.5×10^{-7}			
$e^- \eta$	Belle [77]	401 fb ⁻¹	9.2×10^{-8}	Belle II [40]	50 ab ⁻¹	1.2×10^{-9}
	BABAR [96]	339 fb ⁻¹	1.6×10^{-7}			
	CLEO [97]	4.68 fb ⁻¹	8.2×10^{-6}			
$\mu^- \eta$	Belle [77]	401 fb ⁻¹	6.5×10^{-8}	Belle II [40]	50 ab ⁻¹	8.0×10^{-10}
	BABAR [96]	339 fb ⁻¹	1.5×10^{-7}			
	CLEO [97]	4.68 fb ⁻¹	9.6×10^{-6}			
$e^- \eta'$	Belle [77]	401 fb ⁻¹	1.6×10^{-7}	Belle II [40]	50 ab ⁻¹	1.2×10^{-9}
	BABAR [96]	339 fb ⁻¹	2.4×10^{-7}			
$\mu^- \eta'$	Belle [77]	401 fb ⁻¹	1.3×10^{-7}	Belle II [40]	50 ab ⁻¹	1.2×10^{-9}
	BABAR [96]	339 fb ⁻¹	1.4×10^{-7}			
$e^- f_0(980)$	Belle [73]	671 fb ⁻¹	6.8×10^{-8}	Belle II [40]	50 ab ⁻¹	9.5×10^{-10}
$\mu^- f_0(980)$	Belle [73]	671 fb ⁻¹	6.4×10^{-8}	Belle II [40]	50 ab ⁻¹	9.1×10^{-10}
$e^- \rho^0$	Belle [72]	854 fb ⁻¹	1.8×10^{-8}	Belle II [40]	50 ab ⁻¹	3.8×10^{-10}
	BABAR [101]	451 fb ⁻¹	4.6×10^{-8}			
	CLEO [102]	4.79 fb ⁻¹	2.0×10^{-6}			

Table 4. Cont.

$\tau^- \rightarrow$	Observed Limits			Expected Limits		
	Experiment	Luminosity	UL (obs)	Experiment	Luminosity	UL (exp)
$\mu^- \rho^0$	Belle [72]	854 fb ⁻¹	1.2 × 10 ⁻⁸	Belle II [40]	50 ab ⁻¹	5.5 × 10 ⁻¹⁰
	BABAR [101]	451 fb ⁻¹	2.6 × 10 ⁻⁸			
	CLEO [102]	4.79 fb ⁻¹	6.3 × 10 ⁻⁶			
$e^- \omega$	Belle [72]	854 fb ⁻¹	4.8 × 10 ⁻⁸	Belle II [40]	50 ab ⁻¹	1.0 × 10 ⁻⁹
	BABAR [103]	384 fb ⁻¹	1.1 × 10 ⁻⁷			
$\mu^- \omega$	Belle [72]	854 fb ⁻¹	4.7 × 10 ⁻⁸	Belle II [40]	50 ab ⁻¹	1.4 × 10 ⁻⁹
	BABAR [103]	384 fb ⁻¹	1.0 × 10 ⁻⁷			
$e^- K^{*0}$	Belle [72]	854 fb ⁻¹	3.2 × 10 ⁻⁸	Belle II [40]	50 ab ⁻¹	6.7 × 10 ⁻¹⁰
	BABAR [101]	451 fb ⁻¹	5.9 × 10 ⁻⁸			
	CLEO [102]	4.79 fb ⁻¹	5.1 × 10 ⁻⁶			
$\mu^- K^{*0}$	Belle [72]	854 fb ⁻¹	7.2 × 10 ⁻⁸	Belle II [40]	50 ab ⁻¹	9.3 × 10 ⁻¹⁰
	BABAR [101]	451 fb ⁻¹	1.7 × 10 ⁻⁷			
	CLEO [102]	4.79 fb ⁻¹	7.5 × 10 ⁻⁶			
$e^- \bar{K}^{*0}$	Belle [72]	854 fb ⁻¹	3.4 × 10 ⁻⁸	Belle II [40]	50 ab ⁻¹	6.2 × 10 ⁻¹⁰
	BABAR [101]	451 fb ⁻¹	4.6 × 10 ⁻⁸			
	CLEO [102]	4.79 fb ⁻¹	7.4 × 10 ⁻⁶			
$\mu^- \bar{K}^{*0}$	Belle [72]	854 fb ⁻¹	7.0 × 10 ⁻⁸	Belle II [40]	50 ab ⁻¹	8.5 × 10 ⁻¹⁰
	BABAR [101]	451 fb ⁻¹	7.3 × 10 ⁻⁸			
	CLEO [102]	4.79 fb ⁻¹	7.5 × 10 ⁻⁶			
$e^- \phi$	Belle [72]	854 fb ⁻¹	3.1 × 10 ⁻⁸	Belle II [40]	50 ab ⁻¹	7.4 × 10 ⁻¹⁰
	BABAR [101]	451 fb ⁻¹	3.1 × 10 ⁻⁸			
	CLEO [102]	4.79 fb ⁻¹	6.9 × 10 ⁻⁶			
$\mu^- \phi$	Belle [72]	854 fb ⁻¹	8.4 × 10 ⁻⁸	Belle II [40]	50 ab ⁻¹	8.4 × 10 ⁻¹⁰
	BABAR [101]	451 fb ⁻¹	1.9 × 10 ⁻⁷			
	CLEO [102]	4.79 fb ⁻¹	7.0 × 10 ⁻⁶			
$e^- e^+ e^-$	Belle [78]	782 fb ⁻¹	2.7 × 10 ⁻⁸	Belle II [40]	50 ab ⁻¹	4.7 × 10 ⁻¹⁰
	BABAR [76]	468 fb ⁻¹	2.9 × 10 ⁻⁸			
	CLEO [102]	4.79 fb ⁻¹	2.9 × 10 ⁻⁶			
$\mu^- e^+ e^-$	Belle [78]	782 fb ⁻¹	1.8 × 10 ⁻⁸	Belle II [40]	50 ab ⁻¹	2.9 × 10 ⁻¹⁰
	BABAR [76]	468 fb ⁻¹	2.2 × 10 ⁻⁸			
	CLEO [102]	4.79 fb ⁻¹	1.7 × 10 ⁻⁶			
$e^- \mu^+ \mu^-$	Belle [78]	782 fb ⁻¹	2.7 × 10 ⁻⁸	Belle II [40]	50 ab ⁻¹	4.5 × 10 ⁻¹⁰
	BABAR [76]	468 fb ⁻¹	3.2 × 10 ⁻⁸			
	CLEO [102]	4.79 fb ⁻¹	1.8 × 10 ⁻⁶			
$\mu^- \mu^+ \mu^-$	Belle [78]	782 fb ⁻¹	2.1 × 10 ⁻⁸	Belle II [40]	50 ab ⁻¹	3.6 × 10 ⁻¹⁰
	BABAR [76]	468 fb ⁻¹	3.3 × 10 ⁻⁸			
	LHCb [104]	3 fb ⁻¹	4.6 × 10 ⁻⁸			
	CMS [105]	33 fb ⁻¹	8.0 × 10 ⁻⁸			
	ATLAS [106]	20 fb ⁻¹	3.8 × 10 ⁻⁷			
	CLEO [102]	4.79 fb ⁻¹	1.9 × 10 ⁻⁶			
$e^+ \mu^- \mu^-$	Belle [78]	782 fb ⁻¹	1.7 × 10 ⁻⁸	Belle II [40]	50 ab ⁻¹	2.6 × 10 ⁻¹⁰
	BABAR [76]	468 fb ⁻¹	2.6 × 10 ⁻⁸			
	CLEO [102]	4.79 fb ⁻¹	1.5 × 10 ⁻⁶			
$\mu^+ e^- e^-$	Belle [78]	782 fb ⁻¹	1.5 × 10 ⁻⁸	Belle II [40]	50 ab ⁻¹	2.3 × 10 ⁻¹⁰
	BABAR [76]	468 fb ⁻¹	1.8 × 10 ⁻⁸			
	CLEO [102]	4.79 fb ⁻¹	1.5 × 10 ⁻⁶			

Table 4. Cont.

$\tau^- \rightarrow$	Observed Limits			Expected Limits		
	Experiment	Luminosity	UL (obs)	Experiment	Luminosity	UL (exp)
$e^- \pi^+ \pi^-$	Belle [107]	854 fb ⁻¹	2.3×10^{-8}	Belle II [40]	50 ab ⁻¹	5.8×10^{-10}
	BABAR [108]	221 fb ⁻¹	1.2×10^{-7}			
	CLEO [102]	4.79 fb ⁻¹	2.2×10^{-6}			
$\mu^- \pi^+ \pi^-$	Belle [107]	854 fb ⁻¹	2.1×10^{-8}	Belle II [40]	50 ab ⁻¹	5.6×10^{-10}
	BABAR [108]	221 fb ⁻¹	2.9×10^{-7}			
	CLEO [102]	4.79 fb ⁻¹	8.2×10^{-6}			
$e^- \pi^+ K^-$	Belle [107]	854 fb ⁻¹	3.7×10^{-8}	Belle II [40]	50 ab ⁻¹	7.1×10^{-10}
	BABAR [108]	221 fb ⁻¹	3.2×10^{-7}			
	CLEO [102]	4.79 fb ⁻¹	6.4×10^{-6}			
$\mu^- \pi^+ K^-$	Belle [107]	854 fb ⁻¹	8.6×10^{-8}	Belle II [40]	50 ab ⁻¹	1.2×10^{-9}
	BABAR [108]	221 fb ⁻¹	2.6×10^{-7}			
	CLEO [102]	4.79 fb ⁻¹	7.5×10^{-6}			
$e^- K^+ \pi^-$	Belle [107]	854 fb ⁻¹	3.1×10^{-8}	Belle II [40]	50 ab ⁻¹	7.8×10^{-10}
	BABAR [108]	221 fb ⁻¹	1.7×10^{-7}			
	CLEO [102]	4.79 fb ⁻¹	3.8×10^{-6}			
$\mu^- K^+ \pi^-$	Belle [107]	854 fb ⁻¹	4.5×10^{-8}	Belle II [40]	50 ab ⁻¹	1.2×10^{-9}
	BABAR [108]	221 fb ⁻¹	3.2×10^{-7}			
	CLEO [102]	4.79 fb ⁻¹	7.4×10^{-6}			
$e^- K^+ K^-$	Belle [107]	854 fb ⁻¹	3.4×10^{-8}	Belle II [40]	50 ab ⁻¹	6.5×10^{-10}
	BABAR [108]	221 fb ⁻¹	1.4×10^{-7}			
	CLEO [102]	4.79 fb ⁻¹	6.0×10^{-6}			
$\mu^- K^+ K^-$	Belle [107]	854 fb ⁻¹	4.4×10^{-8}	Belle II [40]	50 ab ⁻¹	1.1×10^{-9}
	BABAR [108]	221 fb ⁻¹	2.5×10^{-7}			
	CLEO [102]	4.79 fb ⁻¹	1.5×10^{-5}			
$e^- K_S^0 K_S^0$	Belle [98]	671 fb ⁻¹	7.1×10^{-8}	Belle II [40]	50 ab ⁻¹	9.7×10^{-10}
	CLEO [100]	13.9 fb ⁻¹	2.2×10^{-6}			
$\mu^- K_S^0 K_S^0$	Belle [98]	671 fb ⁻¹	8.0×10^{-8}	Belle II [40]	50 ab ⁻¹	1.1×10^{-9}
	CLEO [100]	13.9 fb ⁻¹	3.4×10^{-6}			
$e^+ \pi^- \pi^-$	Belle [107]	854 fb ⁻¹	2.0×10^{-8}	Belle II [40]	50 ab ⁻¹	4.6×10^{-10}
	BABAR [108]	221 fb ⁻¹	2.7×10^{-7}			
	CLEO [102]	4.79 fb ⁻¹	1.9×10^{-6}			
$\mu^+ \pi^- \pi^-$	Belle [107]	854 fb ⁻¹	3.9×10^{-8}	Belle II [40]	50 ab ⁻¹	4.5×10^{-10}
	BABAR [108]	221 fb ⁻¹	7.0×10^{-8}			
	CLEO [102]	4.79 fb ⁻¹	3.4×10^{-6}			
$e^+ \pi^- K^-$	Belle [107]	854 fb ⁻¹	3.2×10^{-8}	Belle II [40]	50 ab ⁻¹	7.7×10^{-10}
	BABAR [108]	221 fb ⁻¹	1.8×10^{-7}			
	CLEO [102]	4.79 fb ⁻¹	2.1×10^{-6}			
$\mu^+ \pi^- K^-$	Belle [107]	854 fb ⁻¹	4.8×10^{-8}	Belle II [40]	50 ab ⁻¹	1.2×10^{-9}
	BABAR [108]	221 fb ⁻¹	2.2×10^{-7}			
	CLEO [102]	4.79 fb ⁻¹	7.0×10^{-6}			
$e^+ K^- K^-$	Belle [107]	854 fb ⁻¹	3.3×10^{-8}	Belle II [40]	50 ab ⁻¹	5.8×10^{-10}
	BABAR [108]	221 fb ⁻¹	1.5×10^{-7}			
	CLEO [102]	4.79 fb ⁻¹	3.8×10^{-6}			
$\mu^+ K^- K^-$	Belle [107]	854 fb ⁻¹	4.7×10^{-8}	Belle II [40]	50 ab ⁻¹	9.7×10^{-10}
	BABAR [108]	221 fb ⁻¹	4.8×10^{-7}			
	CLEO [102]	4.79 fb ⁻¹	6.0×10^{-6}			

Table 4. Cont.

$\tau^- \rightarrow$	Observed Limits			Expected Limits		
	Experiment	Luminosity	UL (obs)	Experiment	Luminosity	UL (exp)
$\pi^- \bar{\Lambda}$	Belle [109]	154 fb ⁻¹	1.4×10^{-7}	Belle II [40]	50 ab ⁻¹	5.5×10^{-10}
$\pi^- \Lambda$	Belle [109]	154 fb ⁻¹	7.2×10^{-8}	Belle II [40]	50 ab ⁻¹	5.4×10^{-10}
$\bar{p}^- e^+ e^-$	Belle [110]	921 fb ⁻¹	3.0×10^{-8}	Belle II [40]	50 ab ⁻¹	4.0×10^{-10}
$\bar{p}^- e^+ \mu^-$	Belle [110]	921 fb ⁻¹	2.0×10^{-8}	Belle II [40]	50 ab ⁻¹	4.4×10^{-10}
$\bar{p}^- \mu^+ e^-$	Belle [110]	921 fb ⁻¹	1.8×10^{-8}	Belle II [40]	50 ab ⁻¹	4.4×10^{-10}
$\bar{p}^- \mu^+ \mu^-$	Belle [110]	921 fb ⁻¹	1.8×10^{-8}	Belle II [40]	50 ab ⁻¹	7.4×10^{-10}
	LHCb [36]	1 fb ⁻¹	3.3×10^{-7}			
$p^+ e^- e^-$	Belle [110]	921 fb ⁻¹	3.0×10^{-8}	Belle II [40]	50 ab ⁻¹	3.6×10^{-10}
$p^+ \mu^- \mu^-$	Belle [110]	921 fb ⁻¹	4.0×10^{-8}	Belle II [40]	50 ab ⁻¹	8.3×10^{-10}
	LHCb [36]	1 fb ⁻¹	4.4×10^{-7}			

A beam polarization upgrade of the SuperKEKB e^-e^+ collider can enhance the sensitivity to LFV in τ decays at the Belle II experiment to levels beyond the ones listed in Table 4 and Figure 6. The proposed upgrade [111] will result in $\sim 70\%$ longitudinal polarization of the high energy electron beam, which will influence the angular distribution of the τ decay products in the SM τ -pair backgrounds. The characteristic τ polarization dependence of the helicity angles of the τ decay products with beam polarization can then be used to further suppress the background in, for example, $\tau^- \rightarrow \mu^- \gamma$ searches, where one τ decays to a muon and a photon, while the other τ decays to a pion and a neutrino, the decay channel most sensitive to the polarization of the τ lepton. Similar background suppression can also be obtained with the other decay modes, which vary in their sensitivity to the τ polarization. In general, the maximal discriminating power is obtained by studying the polar angles in the center-of-mass frame times the charge of the τ decay.

The “irreducible background” from $\tau^- \rightarrow \mu^- \nu \bar{\nu} \gamma$ decays are studied in Figure 7 [112]. While the distributions of the backgrounds show marked differences in the case of beam polarization with respect to the case of no beam polarization, the signal distribution modeled by uniform phase-phase does not change with beam polarization. By removing events where the distribution of the irreducible background shows a rising trend near unity, the background can be reduced significantly, corresponding to a small loss in signal efficiency. An optimization study has demonstrated that this would result in approximately a 10% improvement in the sensitivity to LFV. Similar analyses are expected to yield comparable gain in sensitivities for other decay modes.

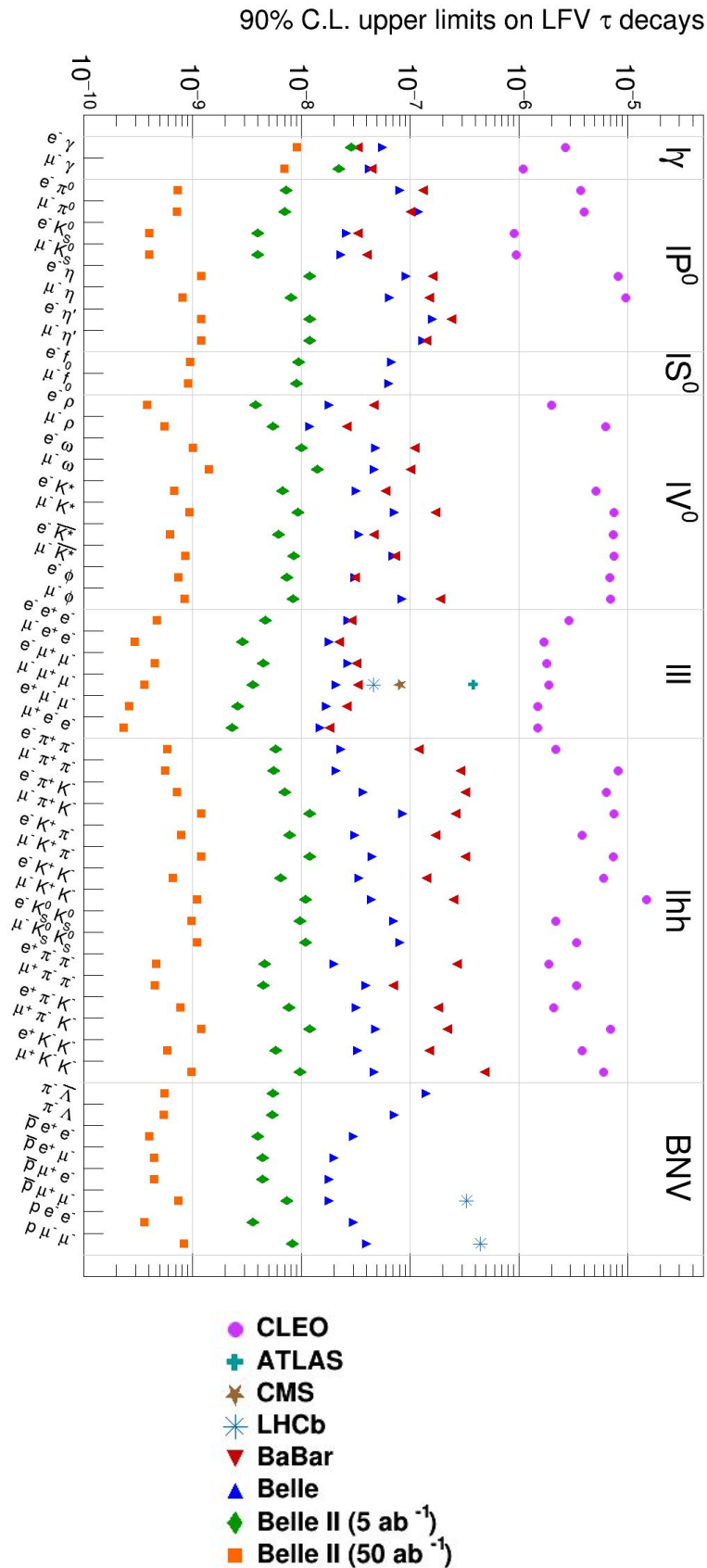


Figure 6. Current status of observed upper limits at CLEO, *BaBar*, Belle, ATLAS, CMS, and LHCb experiments [92] and projections of expected upper limits at the Belle II experiment [40].

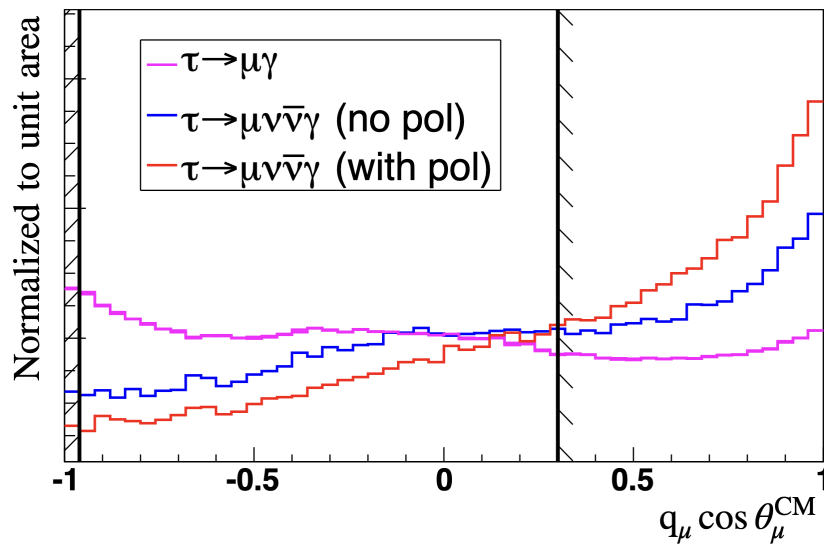


Figure 7. Distribution of the cosine of the signal-side muon multiplied by the muon charge for signal and background events with and without electron beam polarization in the $\tau^- \rightarrow \mu^- \gamma$ search analysis [112].

It is worth noting that the uniform phase space model of the signal distribution is chosen because the underlying theory behind LFV is not known. Different spin-dependent operators are predicted to give significantly different features in the Dalitz plane of final state momenta distributions of, for example, $\tau^- \rightarrow \mu^- \mu^+ \mu^-$ decays [113,114]. One of the most interesting aspects of having the beam polarization is the possibility to distinguish between these different new physics models to understand the helicity structure of the couplings producing LFV in τ decays, once such decays are observed.

Belle II limits will probe predictions from several theoretical models, as listed in Table 1. Some theoretical expectations from different new physics models and improvements on experimental limits over the last few decades for $\tau^- \rightarrow \mu^- \gamma$ [69–71,94,95,115–120] and $\tau^- \rightarrow \mu^- \mu^+ \mu^-$ [36,76,78,102,104–106,115,116,121–126] decays, along with future prospects at Belle II [40], are shown in Figure 8.

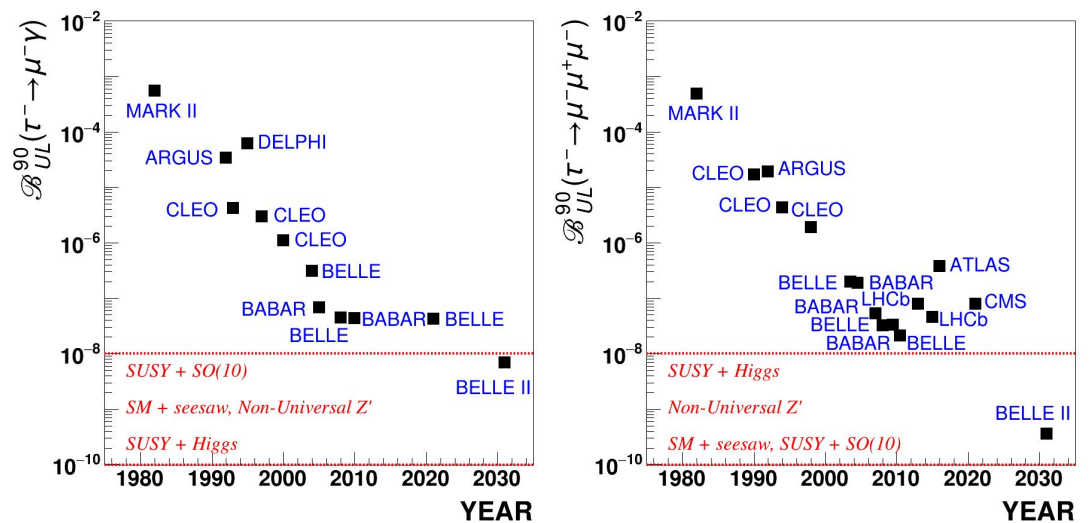


Figure 8. Evolution of experimental bounds on $\tau^- \rightarrow \mu^- \gamma$ [69–71,94,95,115–120] (left) and $\tau^- \rightarrow \mu^- \mu^+ \mu^-$ [36,76,78,102,104–106,115,116,121–126] decays, future prospects at Belle II [40] and some predictions from Table 1.

5. Conclusions

LFV in τ decays are unambiguous signatures of new physics, and are thus of great experimental and theoretical interest. Many models from supersymmetric scenarios to leptoquarks predict LFV in τ decays at experimentally observable rates, which will be probed at Belle II. Searches for LFV in τ decays can discover new physics at the multi-TeV scale by identifying the underlying mechanism beyond the SM, or strongly constrain the flavor structure of TeV-scale extensions beyond the SM [127,128], as discussed in the context of different experimental efforts in Ref. [129]. The first generation B-Factory experiments, Belle and BABAR, saw an order of magnitude improvement on the upper limit on LFV in τ decays from 10^{-6} level down to 10^{-8} level. The Belle II experiment will continue to improve the sensitivity in searches of LFV in τ decays over the next decade. The projected sensitivity at Belle II for LFV in τ decays with 50 ab^{-1} of data is at the 10^{-10} – 10^{-9} level, which constitutes one or two orders of magnitude of improvement over the previous experiments.

Funding: This project was supported by the U.S. Department of Energy under research Grant No. DE-SC0022350.

Institutional Review Board Statement: Not applicable.

Informed Consent Statement: Not applicable.

Data Availability Statement: Not applicable.

Acknowledgments: The author acknowledges fruitful discussions with Kiyoshi Hayasaka, Kenji Inami, John Micheal Roney, Armine Rostomyan, Michel Hernández Villanueva, and many others. Sources of all figures and tables included for discussions have been appropriately cited, and reproduced with permissions from the respective collaborations.

Conflicts of Interest: The author declares no conflict of interest.

References

1. Lee, B.W.; Shrock, R.E. Natural Suppression of Symmetry Violation in Gauge Theories: Muon-Lepton and Electron Lepton Number Nonconservation. *Phys. Rev. D* **1977**, *16*, 1444. [CrossRef]
2. Petcov, S.T. The Processes $\mu \rightarrow e + \gamma$, $\mu \rightarrow e + \bar{e}, \nu' \rightarrow \nu + \gamma$ in the Weinberg-Salam Model with Neutrino Mixing. *Sov. J. Nucl. Phys.* **1977**, *25*, 340; Erratum in *Sov. J. Nucl. Phys.* **1977**, *25*, 698; *Yad. Fiz.* **1977**, *25*, 1336.
3. Pham, X.Y. Lepton flavor changing in neutrinoless tau decays. *Eur. Phys. J. C* **1999**, *8*, 513–516. [CrossRef]
4. Hernández-Tomé, G.; López Castro, G.; Roig, P. Flavor violating leptonic decays of τ and μ leptons in the Standard Model with massive neutrinos. *Eur. Phys. J. C* **2019**, *79*, 84; Erratum in *Eur. Phys. J. C* **2020**, *80*, 438. [CrossRef]
5. Blackstone, P.; Fael, M.; Passemar, E. $\tau \rightarrow \mu\mu\mu$ at a rate of one out of 10^{14} tau decays? *Eur. Phys. J. C* **2020**, *80*, 506. [CrossRef]
6. Cvetič, G.; Dib, C.; Kim, C.S.; Kim, J.D. On lepton flavor violation in tau decays. *Phys. Rev. D* **2002**, *66*, 034008; Erratum in *Phys. Rev. D* **2003**, *68*, 059901. [CrossRef]
7. Ellis, J.R.; Gomez, M.E.; Leontaris, G.K.; Lola, S.; Nanopoulos, D.V. Charged lepton flavor violation in the light of the Super-Kamiokande data. *Eur. Phys. J. C* **2000**, *14*, 319–334. [CrossRef]
8. Ellis, J.R.; Hisano, J.; Raidal, M.; Shimizu, Y. A New parametrization of the seesaw mechanism and applications in supersymmetric models. *Phys. Rev. D* **2002**, *66*, 115013. [CrossRef]
9. Dedes, A.; Ellis, J.R.; Raidal, M. Higgs mediated $B_{s,d}^0 \rightarrow \mu\tau$, $e\tau$ and $\tau \rightarrow 3\mu$, $e\mu\mu$ decays in supersymmetric seesaw models. *Phys. Lett. B* **2002**, *549*, 159–169. [CrossRef]
10. Brignole, A.; Rossi, A. Lepton flavor violating decays of supersymmetric Higgs bosons. *Phys. Lett. B* **2003**, *566*, 217–225. [CrossRef]
11. Masiero, A.; Vempati, S.K.; Vives, O. Seesaw and lepton flavor violation in SUSY SO(10). *Nucl. Phys. B* **2003**, *649*, 189–204. [CrossRef]
12. Hisano, J.; Nagai, M.; Paradisi, P.; Shimizu, Y. Waiting for $\mu \rightarrow e \gamma$ from the MEG experiment. *J. High Energy Phys.* **2009**, *12*, 030. [CrossRef]
13. Fukuyama, T.; Kikuchi, T.; Okada, N. Lepton flavor violating processes and muon g-2 in minimal supersymmetric SO(10) model. *Phys. Rev. D* **2003**, *68*, 033012. [CrossRef]
14. Choudhury, S.R.; Cornell, A.S.; Deandrea, A.; Gaur, N.; Goyal, A. Lepton flavour violation in the little Higgs model. *Phys. Rev. D* **2007**, *75*, 055011. [CrossRef]

15. Blanke, M.; Buras, A.J.; Duling, B.; Poschenrieder, A.; Tarantino, C. Charged Lepton Flavour Violation and (g-2)(mu) in the Littlest Higgs Model with T-Parity: A Clear Distinction from Supersymmetry. *J. High Energy Phys.* **2007**, *5*, 013. [[CrossRef](#)]
16. Davidson, S.; Bailey, D.C.; Campbell, B.A. Model independent constraints on leptoquarks from rare processes. *Z. Phys. C* **1994**, *61*, 613–644. [[CrossRef](#)]
17. Yue, C.X.; Zhang, Y.M.; Liu, L.J. Nonuniversal gauge bosons Z-prime and lepton flavor violation tau decays. *Phys. Lett. B* **2002**, *547*, 252–256. [[CrossRef](#)]
18. Akeroyd, A.G.; Aoki, M.; Sugiyama, H. Lepton Flavour Violating Decays $\tau \rightarrow \bar{\ell}\ell\ell$ and $\mu \rightarrow e\gamma$ in the Higgs Triplet Model. *Phys. Rev. D* **2009**, *79*, 113010. [[CrossRef](#)]
19. Harnik, R.; Kopp, J.; Zupan, J. Flavor Violating Higgs Decays. *J. High Energy Phys.* **2013**, *3*, 26. [[CrossRef](#)]
20. Celis, A.; Cirigliano, V.; Passemar, E. Lepton flavor violation in the Higgs sector and the role of hadronic τ -lepton decays. *Phys. Rev. D* **2014**, *89*, 013008. [[CrossRef](#)]
21. Omura, Y.; Senaha, E.; Tobe, K. Lepton-flavor-violating Higgs decay $h \rightarrow \mu\tau$ and muon anomalous magnetic moment in a general two Higgs doublet model. *J. High Energy Phys.* **2015**, *5*, 28. [[CrossRef](#)]
22. Goudelis, A.; Lebedev, O.; Park, J.H. Higgs-induced lepton flavor violation. *Phys. Lett. B* **2012**, *707*, 369–374. [[CrossRef](#)]
23. Black, D.; Han, T.; He, H.J.; Sher, M. τ - μ flavor violation as a probe of the scale of new physics. *Phys. Rev. D* **2002**, *66*, 053002. [[CrossRef](#)]
24. Babu, K.S.; Kolda, C. Higgs mediated $\tau \rightarrow 3\mu$ in the supersymmetric seesaw model. *Phys. Rev. Lett.* **2002**, *89*, 241802. [[CrossRef](#)]
25. Sher, M. $\tau \rightarrow \mu\eta$ in supersymmetric models. *Phys. Rev. D* **2002**, *66*, 057301. [[CrossRef](#)]
26. Brignole, A.; Rossi, A. Anatomy and phenomenology of mu-tau lepton flavor violation in the MSSM. *Nucl. Phys. B* **2004**, *701*, 3–53. [[CrossRef](#)]
27. Goto, T.; Okada, Y.; Shindou, T.; Tanaka, M. Patterns of flavor signals in supersymmetric models. *Phys. Rev. D* **2008**, *77*, 095010. [[CrossRef](#)]
28. Baldini, A.M.; et al. [MEG Collaboration] Search for the lepton flavour violating decay $\mu^+ \rightarrow e^+\gamma$ with the full dataset of the MEG experiment. *Eur. Phys. J. C* **2016**, *76*, 434. [[CrossRef](#)]
29. Bellgardt, U.; et al. [SINDRUM Collaboration] Search for the Decay $\mu^+ \rightarrow e^+e^+e^-$. *Nucl. Phys. B* **1988**, *299*, 1–6. [[CrossRef](#)]
30. Lopez Castro, G.; Quintero, N. Lepton number violating four-body tau lepton decays. *Phys. Rev. D* **2012**, *85*, 076006; Erratum in *Phys. Rev. D* **2012**, *86*, 079904. [[CrossRef](#)]
31. Gonzalez-Garcia, M.C.; Valle, J.W.F. Enhanced lepton flavor violation with massless neutrinos: A Study of muon and tau decays. *Mod. Phys. Lett. A* **1992**, *7*, 477–488. [[CrossRef](#)]
32. Ilakovac, A. Lepton flavor violation in the standard model extended by heavy singlet Dirac neutrinos. *Phys. Rev. D* **2000**, *62*, 036010. [[CrossRef](#)]
33. Arganda, E.; Herrero, M.J.; Portoles, J. Lepton flavour violating semileptonic tau decays in constrained MSSM-seesaw scenarios. *J. High Energy Phys.* **2008**, *6*, 79. [[CrossRef](#)]
34. Li, W.J.; Yang, Y.D.; Zhang, X.D. $\tau^- \rightarrow \mu^- \pi^0(\eta, \eta')$ decays in new physics scenarios beyond the standard model. *Phys. Rev. D* **2006**, *73*, 073005. [[CrossRef](#)]
35. Pacheco, I.; Roig, P. Lepton flavor violation in the Littlest Higgs Model with T parity realizing an inverse seesaw. *J. High Energy Phys.* **2022**, *2*, 54. [[CrossRef](#)]
36. Aaij, R.; et al. [LHCb collaboration] Searches for violation of lepton flavour and baryon number in tau lepton decays at LHCb. *Phys. Lett. B* **2013**, *724*, 36–45. [[CrossRef](#)]
37. Fuentes-Martin, J.; Portoles, J.; Ruiz-Femenia, P. Instanton-mediated baryon number violation in non-universal gauge extended models. *J. High Energy Phys.* **2015**, *1*, 134. [[CrossRef](#)]
38. Hou, W.S.; Nagashima, M.; Soddu, A. Baryon number violation involving higher generations. *Phys. Rev. D* **2005**, *72*, 095001. [[CrossRef](#)]
39. Banerjee, Sw.; Pietrzyk, B.; Roney, J.M.; Was, Z. Tau and muon pair production cross-sections in electron-positron annihilations at $\sqrt{s} = 10.58$ GeV. *Phys. Rev. D* **2008**, *77*, 054012. [[CrossRef](#)]
40. Aggarwal, L.; et al. [Belle II collaboration] Snowmass White Paper: Belle II physics reach and plans for the next decade and beyond *arXiv* **2022**, arXiv:2207.06307.
41. Akai, K.; Furukawa, K.; Koiso, H. SuperKEKB Collider. *Nucl. Instrum. Meth. A* **2018**, *907*, 188–199. [[CrossRef](#)]
42. Wu, W.; Summers, D. Luminosity and Crab Waist Collision Studies. *arXiv* **2015**, arXiv:1505.06482.
43. Suetsugu, Y.; Shibata, K.; Ishibashi, T.; Kanazawa, K.; Shirai, M.; Terui, S.; Hisamatsu, H. First commissioning of the SuperKEKB vacuum system. *Phys. Rev. Accel. Beams* **2016**, *19*, 121001. [[CrossRef](#)]
44. Ohnishi, Y.; Abe, T.; Adachi, T.; Akai, K.; Arimoto, Y.; Ebihara, K.; Egawa, K.; Flanagan, J.; Fukuma, H.; Funakoshi, Y.; et al. Accelerator design at SuperKEKB. *Prog. Theor. Exp. Phys.* **2013**, *2013*, 03A011. [[CrossRef](#)]
45. Bona, M.; et al. [SuperB collaboration] SuperB: A High-Luminosity Asymmetric e^+e^- Super Flavor Factory. Conceptual Design Report. *arXiv* **2007**, arXiv:0709.0451.

46. Ohnishi, Y. Highlights from SuperKEKB Commissioning for early stage of Nano-Beam Scheme and Crab Waist Scheme. *PoS* **2021**, *ICHEP2020*, 695. [[CrossRef](#)]
47. Abe, T.; et al. [Belle II collaboration] Belle II Technical Design Report. *arXiv* **2010**, arXiv:1011.0352.
48. Altmannshofer, W.; et al. [Belle II collaboration] The Belle II Physics Book. *Prog. Theor. Exp. Phys.* **2019**, *2019*, 123C01; Erratum in *PTEP* **2020**, *2020*, 029201. [[CrossRef](#)]
49. Abashian, A.; et al. [Belle collaboration] The Belle Detector. *Nucl. Instrum. Meth. A* **2002**, *479*, 117–232. [[CrossRef](#)]
50. Abe, R.; et al. [Belle collaboration] The new beampipe for the Belle experiment. *Nucl. Instrum. Meth. A* **2004**, *535*, 558–561. [[CrossRef](#)]
51. Kibayashi, A. Status of the Belle silicon vertex detector. *Nucl. Instrum. Meth. A* **2006**, *569*, 5–7. [[CrossRef](#)]
52. Bevan, A.J.; et al. [BABAR and Belle collaborations] The Physics of the B Factories. *Eur. Phys. J. C* **2014**, *74*, 3026. [[CrossRef](#)]
53. Balagura, V.; Danilov, M.; Dolgoshein, B.; Klemin, S.; Mizuk, R.; Pakhlov, P.; Popova, E.; Rusinov, V.; Tarkovsky, E.; Tikhomirov, I. Study of scintillator strip with wavelength shifting fiber and silicon photomultiplier. *Nucl. Instrum. Meth. A* **2006**, *564*, 590–596. [[CrossRef](#)]
54. Yamada, S.; Itoh, R.; Nakamura, K.; Nakao, M.; Suzuki, S.Y.; Konno, T.; Higuchi, T.; Liu, Z.; Zhao, J. Data Acquisition System for the Belle II Experiment. *IEEE Trans. Nucl. Sci.* **2015**, *62*, 1175–1180. [[CrossRef](#)]
55. Iwasaki, Y.; Cheon, B.; Won, E.; Gao, X.; Macchiarulo, L.; Nishimura, K.; Varner, G. Level 1 trigger system for the Belle II experiment. *IEEE Trans. Nucl. Sci.* **2011**, *58*, 1807–1815. [[CrossRef](#)]
56. Zhou, Q.D.; Yamada, S.; Robbe, R.; Charlet, D.; Itoh, R.; Nakao, M.; Suzuki, S.Y.; Kunigo, T.; Jules, E.; Plaige, E.; et al. PCI-Express Based High-Speed Readout for the Belle II DAQ Upgrade. *IEEE Trans. Nucl. Sci.* **2021**, *68*, 1818–1825. [[CrossRef](#)]
57. Jadach, S.; Ward, B.F.L.; Was, Z. The Precision Monte Carlo event generator KK for two fermion final states in e^+e^- collisions. *Comput. Phys. Commun.* **2000**, *130*, 260–325. [[CrossRef](#)]
58. Ward, B.F.L.; Jadach, S.; Was, Z. Precision calculation for $e^+e^- \rightarrow 2f$: The KK MC project. *Nucl. Phys. B Proc. Suppl.* **2003**, *116*, 73–77. [[CrossRef](#)]
59. Arbuzov, A.; Jadach, S.; Was, Z.; Ward, B.F.L.; Yost, S.A. The Monte Carlo Program KKMC, for the Lepton or Quark Pair Production at LEP/SLC Energies—Updates of electroweak calculations. *Comput. Phys. Commun.* **2021**, *260*, 107734. [[CrossRef](#)]
60. Jadach, S.; Was, Z.; Decker, R.; Kuhn, J.H. The tau decay library TAUOLA: Version 2.4. *Comput. Phys. Commun.* **1993**, *76*, 361–380. [[CrossRef](#)]
61. Chrzaszcz, M.; Przedzinski, T.; Was, Z.; Zaremba, J. TAUOLA of τ lepton decays—Framework for hadronic currents, matrix elements and anomalous decays. *Comput. Phys. Commun.* **2018**, *232*, 220–236. [[CrossRef](#)]
62. Barberio, E.; Was, Z. PHOTOS: A Universal Monte Carlo for QED radiative corrections. Version 2.0. *Comput. Phys. Commun.* **1994**, *79*, 291–308. [[CrossRef](#)]
63. Davidson, N.; Przedzinski, T.; Was, Z. PHOTOS interface in C++: Technical and Physics Documentation. *Comput. Phys. Commun.* **2016**, *199*, 86–101. [[CrossRef](#)]
64. Brandt, S.; Peyrou, C.; Sosnowski, R.; Wroblewski, A. The Principal axis of jets. An Attempt to analyze high-energy collisions as two-body processes. *Phys. Lett.* **1964**, *12*, 57–61. [[CrossRef](#)]
65. Farhi, E. A QCD Test for Jets. *Phys. Rev. Lett.* **1977**, *39*, 1587–1588. [[CrossRef](#)]
66. Antropov, S.; Banerjee, Sw.; Was, Z.; Zaremba, J. TAUOLA update for decay channels with e^+e^- pairs in the final state. *arXiv* **2019**, arXiv:1912.11376.
67. Banerjee, Sw.; Biswas, D.; Przedzinski, T.; Was, Z. Monte Carlo Event Generator updates, for τ pair events at Belle II energies. In Proceedings of the 16th International Workshop on Tau Lepton Physics, Bloomington, IN, USA, 27 September–1 October 2021.
68. Fabre, M. The Dimuon Mass Resolution of the L3 Experiment and its Dependence on the Muon Spectrometer Alignment. Ph.D. Thesis, ETH, Zurich, Switzerland, 1992.
69. Aubert, B.; et al. [BABAR collaboration] Searches for Lepton Flavor Violation in the Decays $\tau^+ \rightarrow e^+\gamma$ and $\tau^+ \rightarrow \mu^+\gamma$. *Phys. Rev. Lett.* **2010**, *104*, 021802. [[CrossRef](#)]
70. Abdesselam, A.; et al. [Belle collaboration] Search for lepton-flavor-violating tau-lepton decays to $\ell\gamma$ at Belle. *J. High Energy Phys.* **2021**, *10*, 19. [[CrossRef](#)]
71. Hayasaka, K.; et al. [Belle collaboration] New Search for $\tau \rightarrow \mu\gamma$ and $\tau \rightarrow e\gamma$ Decays at Belle. *Phys. Lett. B* **2008**, *666*, 16–22. [[CrossRef](#)]
72. Miyazaki, Y.; et al. [Belle collaboration] Search for Lepton-Flavor-Violating tau Decays into a Lepton and a Vector Meson. *Phys. Lett. B* **2011**, *699*, 251–257. [[CrossRef](#)]
73. Miyazaki, Y.; et al. [Belle collaboration] Search for Lepton-Flavor-Violating tau Decays into Lepton and $f_0(980)$ Meson. *Phys. Lett. B* **2009**, *672*, 317–322. [[CrossRef](#)]
74. Fox, G.C.; Wolfram, S. Observables for the Analysis of Event Shapes in e^+e^- Annihilation and Other Processes. *Phys. Rev. Lett.* **1978**, *41*, 1581. [[CrossRef](#)]
75. Zyla P. A.; et al. [PDG collaboration] Review of Particle Physics. *Prog. Theor. Exp. Phys.* **2020**, *2020*, 083C01. [[CrossRef](#)]
76. Lees, J.P.; et al. [BABAR collaboration] Limits on tau Lepton-Flavor Violating Decays in three charged leptons. *Phys. Rev. D* **2010**, *81*, 111101. [[CrossRef](#)]

77. Miyazaki, Y.; et al. [Belle collaboration] Search for lepton flavor violating tau- decays into $\ell^- \eta$, $\ell^- \eta'$ and $\ell^- \pi^0$. *Phys. Lett. B* **2007**, *648*, 341–350. [[CrossRef](#)]
78. Hayasaka, K.; et al. [Belle collaboration] Search for Lepton Flavor Violating Tau Decays into Three Leptons with 719 Million Produced $\tau^+ \tau^-$ Pairs. *Phys. Lett. B* **2010**, *687*, 139–143. [[CrossRef](#)]
79. Helene, O. Upper Limit of Peak Area. *Nucl. Instrum. Meth.* **1983**, *212*, 319. [[CrossRef](#)]
80. Narsky, I.V. Estimation of upper limits using a Poisson statistic. *Nucl. Instrum. Meth. A* **2000**, *450*, 444–455. [[CrossRef](#)]
81. Feldman, G.J.; Cousins, R.D. A Unified approach to the classical statistical analysis of small signals. *Phys. Rev. D* **1998**, *57*, 3873–3889. [[CrossRef](#)]
82. Cousins, R.D.; Highland, V.L. Incorporating systematic uncertainties into an upper limit. *Nucl. Instrum. Meth. A* **1992**, *320*, 331–335. [[CrossRef](#)]
83. Conrad, J.; Botner, O.; Hallgren, A.; Perez de los Heros, C. Including systematic uncertainties in confidence interval construction for Poisson statistics. *Phys. Rev. D* **2003**, *67*, 012002. [[CrossRef](#)]
84. Junk, T. Confidence level computation for combining searches with small statistics. *Nucl. Instrum. Meth. A* **1999**, *434*, 435–443. [[CrossRef](#)]
85. Read, A.L. Presentation of search results: The CL(s) technique. *J. Phys. G* **2002**, *28*, 2693–2704. [[CrossRef](#)]
86. Cowan, G.; Cranmer, K.; Gross, E.; Vitells, O. Asymptotic formulae for likelihood-based tests of new physics. *Eur. Phys. J. C* **2011**, *71*, 1554, Erratum in *Eur. Phys. J. C* **2013**, *73*, 2501. [[CrossRef](#)]
87. Neyman, J. Outline of a Theory of Statistical Estimation Based on the Classical Theory of Probability. *Philos. Trans. R. Soc. Lond Ser. A Math. Phys. Sci.* **1937**, *236*, 333–380. [[CrossRef](#)]
88. Moneta, L.; Belasco, K.; Cranmer, K.S.; Kreiss, S.; Lazzaro, A.; Piparo, D.; Schott, G.; Verkerke, W.; Wolf, M. The RooStats Project. *PoS 2010, ACAT2010*, 057. [[CrossRef](#)]
89. Cranmer, K.; Lewis, G.; Moneta, L.; Shibata, A.; Verkerke, W. HistFactory: A Tool for Creating Statistical Models for Use with RooFit and RooStats 2012. CERN-OPEN-2012-016. Available online: <https://inspirehep.net/literature/1236448> (accessed on 17 August 2022)
90. Cranmer, K.; Kraml, S.; Prosper, H.B.; Bechtle, P.; Bernlochner, F.U.; Bloch, I.M.; Canonero, E.; Chrzaszcz, M.; Cocco, A.; Conrad, J.; et al. Publishing statistical models: Getting the most out of particle physics experiments. *SciPost Phys.* **2022**, *12*, 037. [[CrossRef](#)]
91. Caldwell, A.; Kollar, D.; Kroninger, K. BAT: The Bayesian Analysis Toolkit. *Comput. Phys. Commun.* **2009**, *180*, 2197–2209. [[CrossRef](#)]
92. Amhis, Y.S.; et al. [HFLAV collaboration] Averages of b-hadron, c-hadron, and τ -lepton properties as of 2018. *Eur. Phys. J. C* **2021**, *81*, 226. [[CrossRef](#)]
93. Raidal, M.; Van der Schaaf, A.; Bigi, I.; Mangano, M.L.; Semertzidis, Y.K.; Abel, S.; Albino, S.; Antusch, S.; Arganda, E.; Bajc, B.; et al. Flavour physics of leptons and dipole moments. *Eur. Phys. J. C* **2008**, *57*, 13–182. [[CrossRef](#)]
94. Edwards, K.W.; et al. [CLEO collaboration] Search for neutrinoless tau decays: $\tau \rightarrow e\gamma$ and $\tau \rightarrow \mu\gamma$. *Phys. Rev. D* **1997**, *55*, 3919–3923. [[CrossRef](#)]
95. Ahmed, S.; et al. [CLEO collaboration] Update of the search for the neutrinoless decay tau \rightarrow muon gamma. *Phys. Rev. D* **2000**, *61*, 071101. [[CrossRef](#)]
96. Aubert, B.; et al. [BABAR collaboration] Search for Lepton Flavor Violating Decays $\tau^\pm \rightarrow \ell^\pm \pi^0$, $\ell^\pm \eta$, $\ell^\pm \eta'$. *Phys. Rev. Lett.* **2007**, *98*, 061803. [[CrossRef](#)] [[PubMed](#)]
97. Bonvicini, G.; et al. [CLEO collaboration] Search for neutrinoless tau decays involving pi0 or eta mesons. *Phys. Rev. Lett.* **1997**, *79*, 1221–1224. [[CrossRef](#)]
98. Miyazaki, Y.; et al. [Belle collaboration] Search for Lepton Flavor Violating tau- Decays into $\ell^- K_S^0$ and $\ell^- K_S^0 K_S^0$. *Phys. Lett. B* **2010**, *692*, 4–9. [[CrossRef](#)]
99. Aubert, B.; et al. [BABAR collaboration] Search for Lepton Flavor Violating Decays $\tau^- \rightarrow \ell^- K_S^0$ with the BABAR Experiment. *Phys. Rev. D* **2009**, *79*, 012004. [[CrossRef](#)]
100. Chen, S.; et al. [CLEO collaboration] Search for neutrinoless tau decays involving the K0(S) meson. *Phys. Rev. D* **2002**, *66*, 071101. [[CrossRef](#)]
101. Aubert, B.; et al. [BABAR collaboration] Improved limits on lepton flavor violating tau decays to $\ell^- \phi$, $\ell^- \rho$, $\ell^- K^{*0}$ and $\ell^- \bar{K}^{*0}$. *Phys. Rev. Lett.* **2009**, *103*, 021801. [[CrossRef](#)]
102. Bliss, D.W.; et al. [CLEO collaboration] New limits for neutrinoless tau decays. *Phys. Rev. D* **1998**, *57*, 5903–5907. [[CrossRef](#)]
103. Aubert, B.; et al. [BABAR collaboration] Search for lepton flavor violating decays $\tau^\pm \rightarrow \ell^\pm \omega$ ($\ell = e, \mu$). *Phys. Rev. Lett.* **2008**, *100*, 071802. [[CrossRef](#)]
104. Aaij, R.; et al. [LHCb collaboration] Search for the lepton flavour violating decay $\tau^- \rightarrow \mu^- \mu^+ \mu^-$. *J. High Energy Phys.* **2015**, *2*, 121. [[CrossRef](#)]
105. Sirunyan, A. M.; et al. [CMS collaboration] Search for the lepton flavor violating decay $\tau \rightarrow 3\mu$ in proton-proton collisions at $\sqrt{s} = 13$ TeV. *J. High Energy Phys.* **2021**, *1*, 163. [[CrossRef](#)]
106. Aad, G.; et al. [ATLAS collaboration] Probing lepton flavour violation via neutrinoless $\tau \rightarrow 3\mu$ decays with the ATLAS detector. *Eur. Phys. J. C* **2016**, *76*, 232. [[CrossRef](#)] [[PubMed](#)]

107. Miyazaki, Y.; et al. [Belle collaboration] Search for Lepton-Flavor-Violating and Lepton-Number-Violating $\tau \rightarrow \ell h h'$ Decay Modes. *Phys. Lett. B* **2013**, *719*, 346–353. [[CrossRef](#)]
108. Aubert, B.; et al. [BABAR collaboration] Search for lepton-flavor and lepton-number violation in the decay $\tau^- \rightarrow \ell^\mp h^\pm h'^-$. *Phys. Rev. Lett.* **2005**, *95*, 191801. [[CrossRef](#)]
109. Miyazaki, Y.; et al. [Belle collaboration] Search for lepton and baryon number violating τ^- decays into $\bar{\Lambda}\pi^-$ and $\Lambda\pi^-$. *Phys. Lett. B* **2006**, *632*, 51–57. [[CrossRef](#)]
110. Sahoo, D.; et al. [Belle collaboration] Search for lepton-number- and baryon-number-violating tau decays at Belle. *Phys. Rev. D* **2020**, *102*, 111101. [[CrossRef](#)]
111. Banerjee, Sw.; Roney, J.M. Snowmass 2021 White Paper on Upgrading SuperKEKB with a Polarized Electron Beam: Discovery Potential and Proposed Implementation. *arXiv* **2022** arXiv:2205.12847.
112. Hitlin, D.G.; et al. [SuperB collaboration] New Physics at the Super Flavor Factory. In Proceedings of the 6th superB Workshop, Valencia, Spain, 7–15 January 2008.
113. Matsuzaki, A.; Sanda, A.I. Analysis of lepton flavor violating $\tau^\pm \rightarrow \mu^\pm \mu^\pm \mu^\mp$ decays. *Phys. Rev. D* **2008**, *77*, 073003. [[CrossRef](#)]
114. Dassinger, B.M.; Feldmann, T.; Mannel, T.; Turczyk, S. Model-independent analysis of lepton flavour violating tau decays. *High Energy Phys.* **2007**, *10*, 039. [[CrossRef](#)]
115. Hayes, K.G.; et al. [Mark II collaboration] Experimental Upper Limits on Branching Fractions for Unexpected Decay Modes of the Tau Lepton. *Phys. Rev. D* **1982**, *25*, 2869. [[CrossRef](#)]
116. Albrecht, H.; et al. [ARGUS collaboration] Search for neutrinoless tau decays. *Z. Phys. C* **1992**, *55*, 179–190.
117. Bean, A.; et al. [CLEO collaboration] A Search for $\tau^- \rightarrow \gamma\mu^-$: A Test of lepton number conservation. *Phys. Rev. Lett.* **1993**, *70*, 138–142. [[CrossRef](#)]
118. Abreu, P.; et al. [DELPHI collaboration] Upper limits on the branching ratios $\tau \rightarrow \mu\gamma$ and $\tau \rightarrow e\gamma$. *Phys. Lett. B* **1995**, *359*, 411–421. [[CrossRef](#)]
119. Abe, K.; et al. [Belle collaboration] An Upper bound on the decay $\tau \rightarrow \mu\gamma$ from Belle. *Phys. Rev. Lett.* **2004**, *92*, 171802. [[CrossRef](#)]
120. Aubert, B.; et al. [BABAR collaboration] Search for lepton flavor violation in the decay $\tau \rightarrow \mu\gamma$. *Phys. Rev. Lett.* **2005**, *95*, 041802. [[CrossRef](#)]
121. Bowcock, T.J.V.; et al. [CLEO collaboration] Search for Neutrinoless Decays of the τ Lepton. *Phys. Rev. D* **1990**, *41*, 805. [[CrossRef](#)]
122. Bartelt, J.E.; et al. [CLEO collaboration] Search for neutrinoless decays of the tau lepton. *Phys. Rev. Lett.* **1994**, *73*, 1890–1894. [[CrossRef](#)]
123. Yusa, Y.; et al. [Belle collaboration] Search for neutrinoless decays $\tau \rightarrow 3\ell$. *Phys. Lett. B* **2004**, *589*, 103–110. [[CrossRef](#)]
124. Aubert, B.; et al. [BABAR collaboration] Search for lepton flavor violation in the decay $\tau^- \rightarrow \ell^- \ell^+ \ell^-$. *Phys. Rev. Lett.* **2004**, *92*, 121801. [[CrossRef](#)]
125. Aubert, B.; et al. [BABAR collaboration] Improved limits on the lepton-flavor violating decays $\tau^- \rightarrow \ell^- \ell^+ \ell^-$. *Phys. Rev. Lett.* **2007**, *99*, 251803. [[CrossRef](#)]
126. Miyazaki, Y.; et al. [Belle collaboration] Search for Lepton Flavor Violating tau Decays into Three Leptons. *Phys. Lett. B* **2008**, *660*, 154–160. [[CrossRef](#)]
127. Husek, T.; Monsalvez-Pozo, K.; Portoles, J. Lepton-flavour violation in hadronic tau decays and $\mu - \tau$ conversion in nuclei. *JHEP* **2021**, *1*, 059. [[CrossRef](#)]
128. Cirigliano, V.; Fuyuto, K.; Lee, C.; Mereghetti, E.; Yan, B. Charged Lepton Flavor Violation at the EIC. *J. High Energy Phys.* **2021**, *3*, 256. [[CrossRef](#)]
129. Banerjee, Sw.; Cirigliano, V.; Dam, M.; Deshpande, A.; Fiorini, L.; Fuyuto, K.; Gal, C.; Husek, T.; Mereghetti, E.; Monsálvez-Pozo, K.; et al. Snowmass 2021 White Paper: Charged lepton flavor violation in the tau sector. *arXiv* **2022** arXiv:2203.14919.